Title: The unique molecular recognition features of Siglec-10: structural insights into sialoglycan and antibody interactions

Authors:

Klaudia Sobczak[1], Asier Antoñana-Vildosola[1], Pablo Valverde[2], Maria Alejandra Travecedo[2], Zeinab Jame-Chernaboo[3], Edward N. Schmidt[3], Silvia D´Andrea[4], Eunate Valdaliso-Díez[1], Iker Oyenarte[1], Maria Elena Laugieri[1], Maju Joe[3], Fahima Mozaneh[3], Sung-Yao Lin[3], Alexandre Bosch[1], Maria Jesús Moure[2], Antonio Franconetti[2], So Young Lee[1], Jone Etxaniz-Díaz de Durana[1], Lorena Pérez-Gutierrez[1], Asís Palazón[1,5], Filipa Marcelo[6], Elisa Fadda[4], Francisco Corzana[7], Ana Gimeno[2,5], Matthew S. Macauley[3,8], Jesús Jiménez-Barbero[2,5,9,10*], June Ereño-Orbea[1,5*]

Affiliations:

[1] Cancer Glycoimmunology Lab, Center for Cooperative Research in Biosciences (CIC bioGUNE), Basque Research and Technology Alliance (BRTA), 48160 Derio, Bizkaia, Spain

[2] Chemical Glycobiology lab, Center for Cooperative Research in Biosciences (CIC bioGUNE), Basque Research and Technology Alliance (BRTA), 48160 Derio, Bizkaia, Spain

[3] Department of Chemistry, University of Alberta, 11227 Saskatchewan Drive, Edmonton, Alberta T6G 2G2, Canada

[4] Department of Chemistry, Maynooth University, Maynooth, 99MX VQ, County Kildare, Ireland

[5] Ikerbasque, Basque Foundation for Science, Bilbao, Spain

[6] Applied Molecular Biosciences Unit, Department of Chemistry NOVA School of Science and Technology, 2829-516, Caparica, Portugal

[7] Departament of Chemistry and Instituto de Investigación en Química de la Universidad de La Rioja (IQUR), Universidad de La Rioja, E-26006 Logroño, Spain

[8] Department of Medical Microbiology and Immunology, University of Alberta, Edmonton, Alberta T6G 2E1, Canada

[9] Department of Organic & Inorganic Chemistry, Faculty of Science and Technology, University of the Basque Country, EHU-UPV, 48940 Leioa, Bizkaia, Spain

[10] Centro de Investigacion Biomedica en Red de Enfermedades Respiratorias, 28029 Madrid, Spain

Author list footnotes

*Lead authors: Jesús Jiménez-Barbero[2,4,8,9], June Ereño-Orbea[1,4]

Contact info

Correspondence: June Ereño-Orbea - jereno@cicbiogune.es

Abstract

Siglec-10 is a sialic acid-binding immunoglobulin-like lectin implicated in immune regulation, yet its molecular basis for ligand recognition and functional role in immune modulation remain poorly defined. Here, we present a multidisciplinary study encompassing structural, biochemical, and cellular approaches to elucidate Siglec-10-carbohydrate interactions and function. X-ray crystallography revealed two key arginine residues within the Siglec-10 binding site that interact with the carboxyl group of sialic acid, a canonical R119 and a non-canonical R127, suggesting potential dual contributions to ligand engagement. Saturation Transfer Difference (STD)-NMR confirmed that R119 is essential for binding to sialoglycans, while R127 appears dispensable in interactions with glycans in solution. However, cell-based binding assays using primary human T cells and engineered monocytic lines demonstrated that both arginines (R119 and R127) are critical for cellular recognition, highlighting a more complex mechanism of interaction with the glycocalyx. We further ruled out CD24 as a principal ligand for Siglec-10 on T cells or breast cancer cells, despite high CD24 expression, suggesting the involvement of alternative sialylated glycoproteins or glycolipids. Finally, we show that antibody-mediated blockade of Siglec-10 using S10A mAb restores CAR-T cell cytotoxicity against Siglec-10–expressing target cells, supporting a role for Siglec-10 as an immune checkpoint. These findings identify Siglec-10 as a modulatory receptor with structural and functional features distinct from other Siglec family members and provide a framework for therapeutic targeting in cancer immunotherapy.

Keywords

Siglec, sialic acid, immune checkpoint receptor, crystallography, NMR

Introduction

Aberrant glycosylation is a hallmark of cancer. A prominent example is hypersialylation characterized by an increase in the global expression of sialic acid in cancer, which profoundly alters tumor cell interactions with their microenvironment[1,2,3,4]. In fact, the interactions of sialic acids with the sialic acid-binding immunoglobulin (Ig)-like lectins (Siglecs) family of immune receptors play a pivotal role in immune surveillance within the tumor microenvironment (TME)[5,6,7]. The Siglec family of receptors gathers 15 members, broadly divided into two sub-families based on their conservation across species[8,9]. The potential of the Siglec-sialic acid axis within the TME has been highlighted as a novel immune checkpoint that drives innate and adaptive anti-tumor immune responses[10,11]. Indeed, the inhibitory Siglec receptors[8,9] display structural and signaling motifs similar to those of the well-known inhibitory programmed cell death protein-1 (PD-1)[12,13]. These motifs contain immunoreceptor tyrosine-based inhibitory (ITIM) and ITIM-like motifs that can become phosphorylated and recruit SHP1 and SHP2 phosphatases, thereby dampening immune cell signaling[14].

Amongst the inhibitory Siglecs, Siglec-10 is expressed on antigen-presenting cells (APCs) and presents five extracellular Ig-like domains, comprising one conserved N-terminal variable (V)-set Ig domain and four constant (C)-set Ig domains[11]. The (V)-set Ig domain is responsible for the sialic acid binding properties. Siglec-10 has recently emerged as a modulator of immune responses by expression on tumor-associated macrophages (TAMs)[15]. Different monoclonal antibodies (mAbs) that block the interactions of Siglec-10 and its binding partner(s) promote anti-tumor responses and are currently under evaluation for the treatments of several types of cancer[15,16]. As leading example, ONC-841 is currently in Phase 1 Clinical Trial for the treatment of solid tumors[17]. Although ONC-841 is showing promising outcomes, further data is required to prove the safety of the product. As such, finding other mAbs or small molecules targeting Siglec-10 would improve the outcomes of patients with solid tumors. Additionally, since no Siglec-10 structure has been reported to date, a main issue remains for finding a therapy that is highly specific.

From a molecular perspective, Siglec-10 binds sialylated α2-3 and α2-6 linked glycans through the (V)-set Ig domain[10,18]. Typical binding constants of Siglecs, including Siglec-10 with the Neu_5Ac attached to Gal/GalNAc moieties through α2-3- or α2-6-linkages are rather weak, in the low millimolar range (K_D ranging from 0.1-3 mM), as shown by nuclear magnetic resonance (NMR) experiments for simple sialoglycans[19,20]. Additionally, interactions of Siglec-10 with heavily *O*-glycosylated glycosylphosphatidylinositol (GPI) anchored cell

surface proteins, specifically CD24 and CD52, have also been proposed[15,21,22,23]. One previous study has reported enhanced Siglec-10 binding to sulfated structures on glycan microarrays[24]. However, no cellular or in-solution refined data have been reported for Siglec-10, up to date. It has been recently suggested that carbohydrate sulfation can increase binding affinities for Siglecs-2, -3, -5, -7, -9, and -15[25]. It is important to note that every Siglec displays a conserved canonical arginine residue on the β-strand F of its sialic acid binding site. The canonical Arg is crucial in generating a salt bridge between its guanidine group and the carboxyl group of the Neu_5Ac[10].

Herein, we have determined the first experimental crystal structure, using X-ray crystallography, of the extracellular domain of Siglec-10 in complex with α2-6-sialyllactose. We have also unraveled the binding mode of a variety of sialoglycans to Siglec-10, by combining the X-ray crystal structure with those acquired using NMR techniques, and cell-based assays. Interestingly, the global analysis of the acquired information allowed us to identify a second arginine (R127), close to the canonical one (R119), which is also involved in binding to the carboxyl group of Neu_5Ac. Indeed, the generation of the corresponding mutants and the study of their binding properties have allowed us to detangle the role of the two Arg residues in Siglec-10 interactions with human T cells. In addition, moving forward from the study of glycan binding to biologics, we have delineated the binding epitope on the Siglec-10 V-Ig domain that is recognized by the fragment antigen binding (Fab) of the anti-Siglec-10 blocking Ab (S10A clone)[26]. Binding experiments of recombinant Siglec-10 to human T cells have confirmed the blocking capacity of S10A Ab, while cytotoxicity coculture assays have revealed that binding of S10A Ab to cell surface Siglec-10 has the capability to restore CAR-T cytotoxicity. Overall, our results provide detailed structural and functional insights into molecular recognition features of Siglec-10 at different levels of complexity and suggest that the sialylation profile may regulate these receptor-binding interactions that eventually result in T cell suppression.

Results

Three-dimensional structure of Siglec-10 determined by X-ray crystallography

The extracellular domain of Siglec-10 containing a ternary complex was used for the X-ray crystallographic analysis. The target protein, containing the first two N-terminal Ig domains of Siglec-10 ($Siglec\text{-}10_{d1d2}$), where the sialic acid binding site[10,27] is located was crystallized in

complex with the Fab portion of an anti-Siglec-10 mAb (S10A)[26]. Additionally, a nanobody that recognizes and binds the human kappa light chain (LC) of the Fab[28] was used to stabilize the complex. In agreement with the previous characterization of this IgG antibody[26], the affinity of the S10A Fab was measured to be in the low nanomolar range, with a K_D of 1.1 ± 0.1 nM (**Figure S1**). To facilitate crystallization, the protein complex was first treated with the endoglycosidase H (EndoH) enzyme, which cleaves the high-mannose N-linked glycans present at Siglec-10_{d1d2}. The structure of the ternary complex was solved employing a crystal that diffracted to 2.5 Å resolution and was processed in C2221 space group (**Table S1**), with two molecules in the asymmetric unit (**Figure S2**). The V-Ig (d1) domain is composed of two antiparallel β-sheets formed by β-strands AA'BED and C'CFG β-strands, which are connected by a C41-C101 disulfide linkage, while the second Ig domain (d2) adopts a C1-type fold (**Figure 1a and Figure S3**). The N100 glycan (the remaining GlcNAc moiety after EndoH treatment) is located within the hydrophobic patch at the d1/d2 junction (**Figure 1a, and Figure S3a**), burying 126.9 Å2 of surface area. This N-linked glycan is conserved among Siglecs-2, -4, -5, and -7[29,30,31,32](**Figure S4a**). Interestingly, while in CD22 this N-glycan plays a key role in the correct folding of the protein, in Siglec-10 it does not (**Figure S4b**).

S10A Fab binds primarily at the interface of the two β-sheets of the V-Ig domain (**Figure 1b**), and its binding epitope consists of 886.5 $Å^2$ of buried surface area (BSA), with the light chain (LC) mainly contributing (BSA= 577.1 $Å^2$), as compared to the contribution of the heavy chain (HC) (BSA = 309.4 $Å^2$) (**Figure 1b**). All three of the S10A HC complementarity-determining regions (HCDRs) are involved in the interaction with Siglec-10, providing polar contacts with strands F, C and C'. Alternatively, the light-chain CDRs 1 (LCDR1) and 3 (LCDR3) interact mainly with strand G and the C-C' loop of Siglec-10 (**Figure 1b**).

Next, to understand the binding mode of Siglec-10 with one of its natural ligands, specifically α2-6 sialyllactose ([Neu_5Acα(2-6)Galβ(1-4)Glc] or 6´SL), the crystals of Siglec-10_{d1-d2}-S10A Fab were soaked with 6´SL. Siglec-10 structure in complex with 6´SL ligand was solved at 3.27 Å resolution (**Table S1**). Fittingly, one of the Siglec-10 molecules of the asymmetric unit was found to be bound to 6´SL (**Figure 1c and Figure S2b**). The ligand binding site is formed by strands F and G and loop C–C′ (**Figure 1c**). No electron density was observed for the glucose (Glc) moiety in our crystal structure. This is likely due to a lack of stabilizing interactions of this moiety with Siglec-10. Most of the interactions occur through the *N*-acetylneuraminic acid (Neu_5Ac) portion of the ligand (96.5 Å2 of BSA for Neu_5Ac out of a

total of 243.8 Å2 for $Neu_5Ac\alpha(2\text{-}6)Gal$) (**Table S2**). As for other Siglecs, the electrostatic bond established by the highly conserved arginine residue (R119) and the anionic carboxylate group of the Neu_5Ac moiety[27,33] is clearly observed. However, an additional arginine residue (R127) was also observed at the β-strand G, which is not found in other Siglecs (**Figure S4c**). Remarkably, the negatively charged C1 carboxylate of the Neu_5Ac moiety also interacts with the guanidinium group of this R127 (**Figure 1d**), as well as with that of R119. Additional interactions include N129, which generates hydrogen bonds with the oxygen (O8 and O9) atoms of the Neu_5Ac and T67, which establishes another hydrogen bond with the oxygen (O3) of the Gal moiety (**Figure 1d**).

Additional insights into the binding mode of Siglec-10 to sialoglycans determined by NMR spectroscopy

To characterize the binding of sialoglycans to Siglec-10, we performed STD experiments with Siglec-$10_{d1\text{-}d2}$ wild type (WT) fused to human fragment crystallizable (Fc) from IgG1 (Siglec-10Fc), and 6'-Sialyllactose (6´SL), 3'-Sialyl-*N*-acetyllactosamine (3'SLN), and the sulfated molecule 6-SO_3-6'-SO_3-3'SLN (6-*S*-6'-*S*-3'SLN). The analysis of the STD profiles revealed that all three ligands exhibit nearly identical binding epitopes, and similar to that described for other related Siglecs[19,34] (**Figure 2a**). The *N*-acetyl group of the Neu_5Ac residue exhibits the strongest saturation transfer intensity, closely followed by H6 and H7 of the glycerol chain. These observations suggest that this region of the Neu_5Ac ring is in closer contact at the protein surface, as also revealed by the co-crystal structure. In general, the sialic acid moiety displays high to moderate relative STD effects, while the ones found for the nearby lactose/*N*-acetyllactosamine units are very weak in comparison. Only a few weak-moderate relative STDs (20-40%) could be reported for the Gal unit, suggesting that this moiety might be establishing additional contacts with the protein, while the Glc/GlcNAc unit is expected to be mostly solvent exposed. Overall, the results demonstrate the ability of Siglec-10 to specifically recognize α2-3- and α2-6-sialoglycans, and that the binding is not altered by carbohydrate sulfation.

To further investigate the role of R119 and R127 in binding to sialylated molecules, we introduced R→A or R→K point mutations in Siglec-$10_{d1\text{-}d2}$. These recombinant proteins were still recognized by the S10A Fab, as revealed by BLI (**Figure S5**), suggesting that they are correctly folded and functional. We compared the STD-NMR profiles of the natural ligand 6´SL in the presence of the Siglec-10 wild type (WT), the two single mutants R119A, R127A

and the double mutant R119A/127A (**Figure 2b**). Mutating the canonical R in the R119A and R119A/R127A mutants resulted in no detectable STD intensities (**Figure 2b**), highlighting that the removal of R119 completely abolishes Neu_5Ac-driven binding and underscoring its essential role for the recognition of natural sugars. In contrast, the STD experiments with the single point mutation R127A provided a rather similar ligand epitope map as that found with the WT (**Figure 2b**), supporting that the interaction is very likely to take place in the same way. Interestingly, the binding epitope is similar in relative intensity terms while the absolute STD_0 values are roughly 30% lower for the R127A mutant (**Figure 2b**). This fact suggests that removal of the R127 residue negatively influences the affinity, while the binding pose is essentially maintained. The same approach was undertaken to evaluate the effect of R127A and R119A/R127A point mutations on the binding of 3'SLN and 6-*S*-6'-*S*-3'SLN to Siglec-10Fc (**Figures S6-S9**). As observed for 6´SL, the mutation of R127 residue globally reduced the STD responses, while maintaining the STD profile, again suggesting the effect of this residue on favorably contributing to enhance the binding affinity. On the other hand, the introduction of R119A/R127A point mutations completely abolished the binding, and only non-specific interactions were detected for both ligands (**Figures S6-S9**).

To rationalize our experimental data, we performed 1 µs molecular dynamics (MD) simulations[35] for various Siglec-10/glycan complexes (**Figure S10**). The simulations revealed that the complex formed between Siglec-10 WT and 6´SL ligand is particularly stable, with residue R119 playing a central role in ligand binding. Notably, R127 also interacts with both the carboxylate group of the sialic acid and the hydroxyl group at position O8 of the ligand (**Figures S10a and S10b**). In contrast, MD simulations of the Siglec-10 R127A mutant in complex with 6´SL showed that, while the complex remains stable for approximately the first 350 ns, the ligand eventually dissociates (**Figure S10c**). These results are in full agreement with the experimental observations.

Cell-based binding assays with Siglec-10

To investigate the cellular relevance of R119 and R127 residues in Siglec-10 binding, a series of binding assays were performed using human cells. Initial experiments assessed Siglec-10Fc binding to human $CD4^+$ and $CD8^+$ T cells. Enzymatic removal of surface N- and *O*-linked glycans completely abrogated Siglec-10Fc binding (**Figure 3a** and **Figure S11a**), confirming the glycan-dependence of this interaction. Similarly, treatment with neuraminidase A, which removes both α2-3- and α2-6-linked sialic acids, significantly reduced Siglec-10 interactions

(**Figure 3b** and **Figure S11b**). Specific removal of α2-3-linked sialic acids using neuraminidase S yielded a significant reduction in binding to the human T cells (**Figure 3c** and **Figure S11c**).

To further dissect the contribution of specific sialic acid linkages, we analyzed Siglec-10Fc binding to murine $CD4^+$ and $CD8^+$ T cells deficient in individual sialyltransferases. Binding was preserved in ST3Gal1$^{-/-}$ and ST3Gal4$^{-/-}$ T cells, demonstrating that either a different ST3Gal enzyme creates Siglec-10 ligands or that there is redundancy amongst the ST3Gal enzymes in creating Siglec-10 ligands on murine T cells. On the other hand, binding of Siglec-10Fc was markedly reduced in ST6Gal1$^{-/-}$ T cells, which lack α2-6-linked sialic acids (**Figure 3d**). These findings point to a role for α2-6-sialylated glycoconjugates in mediating Siglec-10 recognition on murine T cells.

To evaluate the individual contributions of the arginine residues to cellular binding, we next assessed the binding of Siglec-10Fc mutants (R119A, R127A, R127K, and the double mutant R119A/R127A) to primary human T cells. All mutations, whether at the canonical R119 or the non-canonical R127, abolished binding to both $CD4^+$ and $CD8^+$ T cells (**Figure 3e** and **Figure S11d**). Strikingly, these findings indicate that both arginine residues are essential for cellular binding.

We also assessed the role of glycan sulfation, a known modulator of Siglec binding [25,36], using a panel of U937 monocytic cells engineered to overexpress sulfotransferases CHST1 and CHST2. We found that Siglec-10Fc binding was reduced in CMAS knockout U937 cells, confirming the necessity of sialic acids at the cell surface (**Figure 3f and Figure S11e**). However, unlike other Siglecs,[25,36] Siglec-10Fc showed no enhanced binding to sulfated glycans (**Figure 3g and Figure S11e**). These data are consistent with the STD-NMR results, indicating a lack of dependence on sulfation for ligand recognition.

Building on these findings, we sought to gain mechanistic insights into how Siglec-10 engages gangliosides at the molecular level. Prior work in liposomal systems identified the disialylated ganglioside GT1b as a good ligand for Siglec-10[37]. To examine the structural basis of this interaction and the role of the two critical arginine residues, we conducted two independent 500-ns molecular dynamics (MD) simulations for Siglec-10 in complex with GT1b embedded in a lipid bilayer. The full-length Siglec-10 structure was modeled using AlphaFold2[35], which produced a highly accurate model with strong agreement to the experimental V-set domain

structure (RMSD = 0.429 Å; **Figure 4** and **Figure S12**). Interestingly, in both MD replicas, GT1b formed stable interactions with both arginines. In particular, R119 primarily engaged the α2-8-linked Neu_5Ac, maintaining >95% occupancy across the simulation in the first replica, while R127 interacted predominantly with the terminal α2-3-linked Neu5Ac (77% occupancy). In the second replica, R119 shifted its interaction to the terminal α2-3-linked Neu_5Ac, indicating flexibility in its engagement with differently linked sialic acids. Notably, R127 consistently maintained interaction with the α2-3 Neu_5Ac across both simulations. These findings support a model in which Siglec-10 utilizes both canonical and non-canonical arginine residues to achieve higher affinity and selective recognition of poly-sialylated epitopes, including gangliosides like GT1b.

Evaluation of CD24–Siglec-10 Binding on Cells

Previous studies have demonstrated that Siglec-10 can recognize CD24 on murine splenocytes[38]. To assess whether CD24 contributes to Siglec-10 binding in a human cancer setting, we first screened a panel of breast cancer cell lines for surface CD24 expression and examined their ability to bind Siglec-10. No correlation was observed between the obtained CD24 surface levels and Siglec-10 binding capacity (**Figure 5a** and **Figure S13**), suggesting that CD24 expression alone is not sufficient to confer binding.

We next tested whether CD24 functionally contributes to Siglec-10 interactions by performing binding assays in the presence of a CD24-blocking monoclonal antibody (clone SN3)[15]. Antibody-mediated blockade of CD24 did not diminish Siglec-10 binding to breast cancer cells (**Figure 5b**), further supporting the notion that CD24 is not a key Siglec-10 ligand in this setting.

Given that CD24 is known to be highly expressed on human T cells[39,40,41], we also evaluated its role in Siglec-10 binding on activated T cells isolated from peripheral blood mononuclear cells (PBMCs). While CD24 was robustly expressed (**Figure 5c**), blockade with the SN3 antibody had no effect on Siglec-10 binding (**Figure 5c**). To test whether enforced CD24 expression could enhance Siglec-10 binding, we generated a CD24-overexpressing Jurkat T cell line. However, these cells showed no increase in Siglec-10 binding compared to parental controls (**Figure 5d**).

Together, these results demonstrate that despite high CD24 expression in various cellular contexts, CD24 does not mediate or enhance Siglec-10 binding in breast cancer or T cell models tested here. This evidence suggests that other sialoglycoproteins are likely responsible for Siglec-10 engagement in these settings.

Siglec-10 blockade restores CAR T cell cytotoxicity

To explore whether Siglec-10 functions as a checkpoint inhibitor of T cell effector activity, we employed an antigen-specific *in vitro* cytotoxicity assay (**Figure 6a**). THP-1 myeloid cells were engineered to express a non-signaling truncated form of CD19 (CD19t), serving as a model antigen, and further transduced to overexpress Siglec-10 (**Figure S14a**). In parallel, primary human T cells were transduced with a clinically validated anti-CD19 chimeric antigen receptor (CAR) construct to enable antigen-specific killing (**Figure S14b**).

The cytotoxic activity of CAR-T cells against THP-1-CD19 cells with or without Siglec-10 expression was tested by flow cytometry. The results showed that overexpression of Siglec-10 on target cells significantly impairs CAR-T cell-mediated killing **(Figure 6b).** To further evaluate the ability of Siglec-10 to inhibit T cell cytotoxicity, we repeated the cytotoxicity assay in the presence of the S10A IgG4 mAb. S10A IgG4 could block the interaction between Siglec-10 and sialoglycans present on $CD4^+$ and $CD8^+$ T cells **(Figure 6c),** consistent with the predictions based on our co-crystal structure. To assess antibody engagement and internalization, a pH-sensitive pHrodo Red dye (Thermo Fisher) was used, which fluoresces in acidic compartments, such as lysosomes. Flow cytometry analysis confirmed internalization of S10A mAb upon Siglec-10 binding, and this result was further validated by using confocal microscopy (**Figure 6d**). Strikingly, treatment with the S10A mAb restored CAR-T cell cytotoxicity specifically against Siglec-10-expressing target cells (**Figure 6e**), demonstrating that the suppressive effect of Siglec-10 is reversible and antibody-dependent.

Discussion

Siglec-10 is a member of the Siglec family that modulates immune responses through recognition of sialoglycans. Despite its functional relevance in immune tolerance and tumor immune evasion, the structural and molecular basis of Siglec-10 ligand recognition has remained poorly defined. Here, we have combined structural biology, NMR spectroscopy,

mutagenesis, and cellular binding assays to provide a comprehensive picture of the glycan-binding interface of Siglec-10 and its functional implications in immune cell recognition.

The analysis of our crystal structure of Siglec-10 in complex with 6´SL has revealed the presence of two Arg residues—one canonical (R119) and one non-canonical (R127)—within the carbohydrate recognition domain of Siglec-10. This dual-arginine display is previously unidentified in Siglecs and suggests a potential cooperative role in sialic acid engagement. STD-NMR data demonstrated that mutation of the canonical R119 residue alone is sufficient to abolish binding to trisaccharide glycan ligands in solution.

In contrast, our cell-based assays revealed a more complex picture: mutation of either R119 or R127, completely eliminated Siglec-10 binding to human $CD4^+$ and $CD8^+$ T cells. These findings indicate that although R127 is dispensable for recognition of minimal glycan motifs *in vitro*, it is essential for glycan engagement in the cellular context. One possible explanation is that R127 helps stabilize or orient the CRD for productive interaction with complex or multisialylated glycans on the cell surface, such as disialylated gangliosides. This interpretation is further supported by our molecular dynamics (MD) simulations of Siglec-10 bound to the GT1b ganglioside, which underscore the importance of R127 for maintaining stable Siglec-10/glycan interactions under physiologically relevant conditions. Other examples of non-canonical binding sites have also been described for other Siglecs. For instance, Siglec-7 has been shown to rely on both canonical and non-canonical residues for the recognition of di- and tri-sialylated structures[42].

The glycan dependency of Siglec-10 binding was further investigated using enzymatic treatments, genetically modified cell models, and sialyltransferase-deficient mice. Enzymatic removal of N- and *O*-linked glycans from human T cells completely abolished Siglec-10 binding, confirming that the interaction is glycan-dependent. Additionally, treatment with α2-3-specific neuraminidase significantly reduced binding. In murine T cells Siglec-10 binding was markedly reduced in ST6Gal1$^{-/-}$ cells, which lack α2-6-linked sialic acids, while binding was preserved in ST3Gal1$^{-/-}$ and ST3Gal4$^{-/-}$ cells. This combination of enzymatic digestion and genetic models point that both α2-3- and α2-6-sialylations are required in T cells, although there might be species-specific differences with α2-3-sialylation dependency on human T cells. However, the experimental conditions used in the two systems are different, each with their own drawbacks. For instance, α2-6-linked sialic acids can adopt conformations that render

them less accessible, such as hairpin-like structures, which may limit the efficiency of enzymatic cleavage. In contrast, terminal α2-3-linked sialic acids are generally solvent-exposed, possibly explaining the more pronounced effects observed with α2-3-specific neuraminidase treatment in human cells. Moreover, genetic knockout models must be interpreted with caution, as compensatory pathways or broader alterations in the glycome architecture may influence binding outcomes in ways that are not immediately apparent.

Further supporting the requirement for sialylated ligands, Siglec-10 binding was substantially reduced in CMAS-deficient U937 cells, which lack *de novo* sialic acid biosynthesis. This result confirms that sialic acids are essential for Siglec-10 interactions across different cellular contexts. Moreover, in contrast to several other Siglec family members, Siglec-10 binding was not enhanced by overexpression of the sulfotransferases CHST1 or CHST2, indicating that sulfation does not play a major role in modulating its ligand affinity. This observation is consistent with the STD-NMR data, which revealed minimal interaction with sulfated glycan epitopes.

In light of previous studies suggesting CD24 as a key Siglec-10 ligand in cancer, we investigated whether CD24 mediates Siglec-10 interactions in our experimental system. Although we confirmed high CD24 expression on both T cells and multiple breast cancer cell lines, neither antibody-mediated CD24 blockade nor CD24 overexpression in Jurkat cells had any effect on Siglec-10 binding. These results suggest that CD24 does not play a major role in Siglec-10 recognition in these cellular contexts, in contrast with earlier studies that implicated CD24 in Siglec-10 signaling within tumor-associated macrophages. Consistent with our findings, a recent CRISPR activation (CRISPRa) screen in K-562 cells identified N-linked glycans terminating in α2-3- or α2-6-linked sialic acids as preferred Siglec-10 ligands. Notably, CD24 was not among the ligands identified in this screen, further supporting the notion that other glycoproteins may serve as dominant Siglec-10 ligands in these settings[43].

This discrepancy points to the possibility of context- or cell type-specific ligand repertoires for Siglec-10. It is conceivable that CD24 contributes to Siglec-10 engagement only in specific immunological environments or under distinct post-translational modifications, such as fucosylation or clustered *O*-glycosylation patterns, which may not be present in our models. Additionally, previous studies have proposed that the high-mobility group box 1 (HMGB1) protein facilitates the formation of a ternary complex involving Siglec-10 and either CD24[44] or

CD52[45]. The absence of such accessory molecules in our system may further explain the lack of detectable Siglec-10/CD24 interaction.

Taken together, our results highlight the complex interplay between structural determinants and cellular context for Siglec-10/ligand recognition. The dual-arginine display of Siglec-10 may confer specificity for diverse glycan ligands in different environments. The lack of sulfation dependence and the exclusion of CD24 as a universal ligand suggest that Siglec-10 recognizes distinct, yet-to-be-identified glycoproteins or glycolipids on human immune and tumor cells. Future studies using glycoproteomic or ligand-capture strategies will be essential to fully define the endogenous ligands of Siglec-10 and their relevance in health and disease.

In any case, our data support the role for Siglec-10 as a glyco-immune checkpoint receptor that can modulate T cell effector function. Additionally, overexpression of Siglec-10 on target cells did suppress CAR-T cell cytotoxicity, while obstruction of Siglec-10 with the blocking S10A mAb restored and markedly enhanced CAR-T cell-mediated killing in a Siglec-10-dependent manner. This fact suggests that inhibitory signals mediated by Siglec-10 require engagement with sialylated ligands on effector T cells. These findings not only position Siglec-10 as a potential immune checkpoint receptor but also supports the rationale for Siglec-10 blockade as a strategy to enhance T cell-based immunotherapies, including CAR-T cell approaches.

Materials and Methods

Primary human T cells

T cells were obtained from buffy coats of healthy donors (Biobanco Vasco, BIOEF) after ethical approval (PI + CES-BIOEF 2019-08). Briefly, PBMCs were separated by gradient differentiation using FicollHistopaque (17-1440-03, Fisher scientific), and CD3+ T cells were purified by negative selection using EasySep™ Human T Cell Enrichment Kit (Stemcell) following manufacturer's instructions. Purity was confirmed by flow cytometry to be >95%. T cells were then activated with anti-CD3/CD28 Dynabeads (11131D, Thermo Fisher) in CST OpTimizer medium (A1048501, Gibco) supplemented with IL-2 at 100 IU/mL (130-097-743, Miltenyi Biotec).

CAR constructs

Second generation CARs targeting CD19 were developed in our laboratory. The anti-CD19 scFv was derived from the FMC63 monoclonal antibody (REF Nicholson Mol. Immunol. 34,

1157–1165 (1997)). The CAR construct included CD8a signaling peptide, the anti-CD19 scFv, the CD8alpha hinge/transmembrane domain, 4-1BB intracellular domain, and CD3z intracellular domain. To facilitate CAR-T cell identification and selection, a T2A self-cleaving peptide followed by truncated NGFR was incorporated into the CAR coding sequence. The construct was cloned into a third-generation lentiviral vector under the control of the EF1a constitutive promoter and synthesized by Genscript.

Lentivirus production and titration

To generate lentiviral particles, 5×10^6 293T cells were seeded in a 100 mm dish. Twenty-four hours after cell seeding, cells were transfected using a mix of lentiviral plasmids (three plasmids were used for 2nd generation lentivirus used for THP-1 cell line transduction: transfer plasmid; 5 µg, psPAX2 (Addgene #12260; 4 µg) and VSV-G (Addgene #8454; 1.5 µg. In the case of 3rd generation lentivirus for transduction of primary T cells, four plasmids were used: transfer plasmid; 6.9 µg, RRE 3.4 µg, REV 1.7 µg and VSV 2.0 µg)) and jetPEI transfection reagent (Polyplus) following manufacturer's instructions. After 48 h, lentiviral particles were harvested from the supernatant, filtered through a 0.45 µm filter (VWR) and concentrated using LentiX contentrator (Takara) at a 3:1 ratio at 4 °C overnight. Lentiviral particles were then concentrated by centrifugation at 1500g for 45 min, aliquoted, and stored at −80 °C until use.

Lentivirus was tittered using Jurkat cells. Briefly, $5x10^4$ Jurkat cells were plated in 96-well plates in complete RPMI medium containing serial dilutions of thawed lentivirus (e.g. 3-fold serial dilutions from 3:100 to 3:100,000) and 8 mg/ml polybrene. After 48 hours, cells were analyzed for transgene expression by flow cytometry. Virus titer was calculated according to the following formula: Titer (pfu/ml) = [($5x10^4$) * (%positive cells) / 100] / [Volume of virus added (ml)].

Human T cell transduction

For CAR lentiviral transduction, $CD3^+$ T cells were initially activated with CD3/CD28 Dynabeads in OpTmizer medium supplemented with human IL-2. Two days post-activation, these cells were transduced with the desired lentivirus at a multiplicity of infection (MOI) of 6 in the presence of 8 µg/mL Polybrene (Merck). Spinoculation was performed at 800g for 1 hour at 32°C and cells were maintained in complete OpTmizer media containing IL-2 at a density of 0.5×10^6 cells/mL, with fresh media replenished every 2-3 days. Four days after transduction, beads were magnetically removed, and CAR-T cells were isolated using the

EasySep Human CD271 Positive Selection Kit II (StemCell Technologies). These selected cells were expanded until days 10–12 post-activation, then cryopreserved in FBS with 10% DMSO. The purity of the CAR-T cells was routinely verified to be >85% by flow cytometry.

Cell lines

HEK293F (R79007, Thermo Fisher) and HEK293S (CRL-3022) cells were grown at 37°C, 70% humidity 8% CO2 at 130 rpm in Freestyle media (12338018, Thermo Fisher). Jurkat, THP-1 (WT and THP-1-CD19t-GFP transduced) (TIB-202, ATCC) and U937 (the U937-CHST1, U937-CHST2 and U937-CMAS KO cell lines were generated according to a previously published protocols[36,46]) cells were grown in RPMI (15140122, Gibco) medium. The HEK293T Lenti-X (632180, Takara Bio Inc.) cell line was maintained in DMEM (41966-029, Gibco). Both, RPMI and DMEM media were supplemented with 10% heat-inactivated FBS (A3840002, ThermoFisher) and 1% penicillin/streptomycin mix (pen/strep) (15140122, ThermoFisher). THP-1 cell line was grown in T25 flasks (156340, ThermoFisher), whereas HEK293T LentiX were maintained in T75 flasks (156472, ThermoFisher), and passed twice a week. To keep optimal conditions for cell culture, the THP-1 and HEK293T LentiX cells were kept at 37°C, 5% CO2, and 70% humidity.

For cytotoxicity experiments, THP-1 cell line was transduced with a lentivirus expressing luciferase-EGFP and CD19 target antigen followed by T2A-puromycin resistance gene and was then sorted for $CD19^{+}GFP^{+}$ cells. Following, the THP-1-GFP-CD19 cell line was transduced with various Siglec-10 constructs, specifically Siglec-10 WT, R119A, R127A, R119/127A and ITIM mut followed by a T2A-blasticidin resistance gene, generating five different Siglec-10 expressing THP-1-GFP-CD19 cell lines.

Mouse Strains

All mice used in this study were on a C57BL/6J genetic background. The following strains were obtained from The Jackson Laboratory: C57BL/6J (Strain #: 000664), $CD4^{Cre}$ (Strain #: 022071), $ST6Gal1^{fl/fl}$ (Strain #: 006901). To generate the $ST6Gal1^{fl/fl}$ × $CD4^{Cre}$ mice, $ST6Gal1^{fl/fl}$ animals were crossed with $CD4^{Cre}$ mice. Genotyping was performed by PCR using DNA extracted from ear notch tissue. For the ST6Gal1 locus, the forward primer 5'-TCAGCAGCCTGGGGTTAAGT-3' and reverse primer 5'-CCTGTACACTGAATGGTGGACTGTGG-3' were used. The wild-type allele generated a 1115 bp product, while the floxed allele produced a 900 bp product. ST3Gal1 and ST3Gal4

knockout mice were generously provided by Dr. Jamey Marth (Sanford Burnham Prebys Medical Discovery Institute, USA).

Construct design of Siglec-10 extracellular domain and S10A proteins

The DNA encoding the first Ig domains of the extracellular domain (d1-d2) of human Siglec-10 (UniprotKB Q96LC7, residues 17-238) fused to 6xHis tag , codon optimized for expression in human cells and cloned into pHLsec vector between and KpnI restriction sites. The DNA encoding human Siglec-$10_{d1–d2}$ WT and R119A, R127A, R127K and R119A/R127A mutants fused to the human IgG1 Fc region (UniprotKB P01857, residues 99–330) and with a C-terminal 6x His tag, were subcloned between XbaI and AfeI restriction sites into pcDNA 3.4 (Invitrogen) and codon optimized for expression in human cells. For the S10A Fab, the heavy (residues 1-214) and light (residues 1–224) chains were synthesized and cloned into pHLsec vector between and KpnI restriction sites. For the S10A IgG4 mAb, the light chain used was the same as for S10A Fab, as described above, whereas the heavy chain was fused with the IgG4 backboune (residues 1-327) and was sysnthesized and cloned into pcDNA3.1 vector between Xbal and AgeI restriction sites. All plasmids were synthesized by GenScript.

Protein expression and purification

Siglec-10_{d1-d2} and Siglec-10Fc (WT and mutants) constructs were transiently transfected using HEK293F/S suspension cells. Cells were split in 500 mL cultures at 1.0×10^6 cells/mL. The DNA: FectoPRO transfection reagent solution (101000007, Polyplus) was then added directly to the cells, and cells were incubated at 37 °C, 130 rpm, 8% CO_2 and 70% humidity for 6–7 days. Supernatants were passed through a His-Trap Ni-NTA (17528601, GE Healthcare) and then separated on a Superdex 200 Increase size exclusion column (GE28-9909-44, GE Healthcare) in 20 mM Tris pH 9.0 (PHG0002, Sigma-Aldrich), 300 mM NaCl (S9888, Sigma-Aldrich) buffer to achieve size homogeneity.
The heavy and light chains of S10A Fab and S10A IgG4 were co-expressed at 2(heavy):1(light) ratio using HEK293F cells as described elsewhere[59]. S10A Fab/IgG4 were purified using KappaSelect affinity (17545812, GE Healthcare). Fractions containing protein were pooled and run on a Superdex 200 Increase gel filtration column to obtain purified samples.

Siglec-10_{d1-d2}–S10A Fab complex was obtained by transiently co-transfecting Siglec-10_{d1-d2} with the LC and HC of S10A Fab using HEK293S suspension cells at 2:2:1 ratio, respectively.

Expression was achieved following the same procedure described for Siglec-10 alone. The protein complex was purified using HiTrap Ni-NTA column (GE Healthcare) followed by Superdex 200 Increase size exclusion column (GE Healthcare). In order to facilitate crystallization, the complex was treated with endoglycosidase H (EndoH), which cleaves high-mannose N-linked glycans present on N100 residue of Siglec-10_{d1d2}. The complex was then incubated for 2hrs at RT with a 100x molar excess of V_HH nanobody (REF) and then the ternary complex was purified using Superdex 200 Increase size exclusion column (GE Healthcare) in 20 mM Tris pH 9.0, 300 mM NaCl buffer to achieve size homogeneity.

Ligands

3'SLN and 6'SL were kindly provided by Prof Rob Field from the Manchester Institute of Biotechnology in the UK. The detailed synthesis of 6-SO_3-6'-SO_3-3'SLN can be found in *supplementary methods* and **Figures S15-19**.

Crystallization, X-ray diffraction data collection, and 3D structure determination

Purified Siglec-10_{d1d2}-S10A-V_HH complex was concentrated to 13 mg/mL in a buffer containing 20 mM Tris pH 9.0 and 300 mM NaCl. Crystals were obtained by hanging drop vapor diffusion at 291 K in 0.16M ammonium sulfate, 0.08M sodium acetate and 20 % (v/v) PEG 4000 in 24-well plates after mixing 1 µL of the protein complex and 1 µL of the precipitant solution. Crystals were cryo-preserved by soaking them in mother liquor solution containing 25 % glycerol and flash frozen in liquid nitrogen. X-ray diffraction data was collected at the DLS IO4 synchrotron beamline at DIAMOND (UK). Data was processed using autoPROC in C2221 space group at 2.4 Å resolution. The structure was determined by molecular replacement using the Siglec-15 (PDB ID: 7ZOZ) and the light and heavy chains of 5G12 Fab (PDB ID: 7ZOR) as search model in Phaser.

Crystals of Siglec-10–S10A-V_HH-α2-6SL complex were obtained by soaking of the already existing crystals of Siglec-10–S10A-V_HH complex with 100 µM of the ligand (α2-6 sialylactose). The ligand solution was added to the crystal containing drop at a 1:3 protein: ligand ratio.The soaked crystals were then collected and flash frozen in crystallization buffer containing 25% glycerol at different time-points (1 min, 5 mins, and 1 hour). X-ray diffraction data was collected at the DLS IO4 synchrotron beamline at DIAMOND (UK). Data was processed using autoPROC in C2221 space group at 3.27 Å resolution.

All structures were refined by manual building in Coot and using phenix.refine. PyMOL was utilized for structure analysis and figure rendering. All buried surface area values reported were calculated using EMBL-EBI PDBePISA. The crystal structures of Siglec-10_{d1d2}/S10A and Siglec-10/S10A/α2-6SL complex reported in this manuscript have been deposited in the Protein Data Bank, www.rcsb.org with PDB ID 9R7P and 9R8E, respectively.

Biolayer interferometry

The binding affinities of S10A Fab to Siglec-10Fc was measured by BLI using the Octet R8 BLI system (Sartorius). AHC2 biosensors (18-5142, Sartorius) were hydrated in 1× kinetics buffer (PBS, pH 7.4, 0.002 % Tween, 0.01 % bovine serum albumin (BSA)) and loaded with 20 ng/µL of Siglec-10Fc for 200 s at 1000 rpm. Biosensors were then transferred into wells containing 1× kinetics buffer to baseline for 200 s before being transferred into wells containing a serial dilution of Fab starting at 120 nM and decreasing to 3.75 nM. The 200 s association phase was subsequently followed by a 200 s dissociation step in 1× kinetics. Analysis was performed using the Octet software (Sartorius), with a 1:1 fit model. All experiments were repeated in triplicate, values were averaged, and standard errors were calculated.

NMR experiments

Ligand assignment and STD-NMR experiments with 6´SL were carried out on an 800 MHz Bruker spectrometer equipped with a triple-channel cryoprobe (Bruker, Billerica, MA, USA). All STD experiments were acquired at 298 K in all cases using an in-house pulse sequence.
STD-NMR experiments with 3'SLN and the sulfated 6-S-6'-S-3'SLN molecules were acquired on a Bruker Avance III 600 MHz spectrometer equipped with a 5-mm inverse detection triple-resonance cryogenic probe head with z-gradients and ligand assignment NMR experiments were acquired on a Bruker Avance 500 MHz equipped with a triple channel TXI probe. All spectra were acquired at 288 K. Detailed experimental procedures are provided in the *supporting materials and methods.*

MD Simulations of the Siglec-10 and 6´SL complexes

MD simulations were carried out with AMBER 22[47], implemented with ff14SB, which is an evolution of the Stony Brook modification of the Amber 99 force field force field (ff99SB)[48] and GLYCAM06[49] force fields. The structure of Siglec-10 was predicted using Alphafold[50] the

glycopeptides were build-up with Carbohydrate Builder (https://glycam.org/cb/) and the complexes were generated using Protenix Server (https://protenix-server.com/login). Each complex was immersed in a 10 Å water box with TIP3P[51] water molecules and charge neutralized by adding explicit counter ions (Na+). A two-stage geometry optimization approach was performed. The first stage minimizes only the positions of solvent molecules and ions, and the second stage is an unrestrained minimization of all the atoms in the simulation cell. The systems were then gently heated by incrementing the temperature from 0 to 300 K under a constant pressure of 1 atm and periodic boundary conditions. Harmonic restraints of 30 kcal·mol–1 were applied to the solute, and the Andersen temperature coupling scheme[52]. was used to control and equalize the temperature. The time step was kept at 1 fs during the heating stages, allowing potential inhomogeneities to self-adjust. Water molecules are treated with the SHAKE algorithm such that the angle between the hydrogen atoms is kept fixed. Long-range electrostatic effects are modelled using the particle-mesh-Ewald method[53]. An 8 Å cutoff was applied to Lennard-Jones and electrostatic interactions. Each system was equilibrated for 2 ns with a 2-fs time step at a constant volume and temperature of 300 K. Production trajectories were then run for additional 1.0 μs under the same simulation conditions.

MD Simulations of the Siglec-10 in complex with GT1b

The 3D structure of full-length Siglec-10 ECD was generated with AlphaFold-2 (AF2)[50] (AlphaFold Protein Structure Database number AF-Q96LC7)[54]. GT1b ganglioside from GlyTouCan (G08648UJ) was used. The equilibrium structure of the GT1b was sourced from the GlycoShape server[55,56]. The starting conformation of the complex was built to complement the 3D structure of GT1b, with an orientation selected to maximize the number of arginine residues engaging the trisialylated GT1b headgroup. Accordingly, the terminal α2-8-linked Neu5Ac was positioned to interact with the canonical R119, while R127, and R80 aligned to interact the internal and terminal α2-3-linked Neu5Ac residues, respectively. The complex was embedded in a symmetric 130 Å × 130 Å lipid bilayer composed of 60% 1,2-distearoyl-sn-glycero-3-phosphocholine (DSPC) and 40% cholesterol (CHL1) using the CHARMM-GUI Membrane Builder tool[57]. All molecular dynamics (MD) simulations were conducted with AMBER 22, using the CHARMM36m force field to parameterize the protein, lipids, and glycans. The system was first energy minimized for 5000 steps (2500 steps of steepest descent

followed by 2500 steps of conjugate gradient minimization). Equilibration was performed following the CHARMM-GUI protocol[58], consisting of six steps. Positional restraints of 10 kcal/mol·Å² were initially applied to the system and were gradually reduced during the NPT equilibration phase, progressively lowered to 5 kcal/mol·Å² for the protein and 2.5 kcal/mol·Å² for the membrane until they were completely removed. Temperature was maintained at 315.15 K using Langevin dynamics with a friction coefficient (gamma_ln) set to 1.0 ps − 1. and pressure was controlled semi-isotropically at 1 atm using the Berendsen barostat. Periodic boundary conditions were applied throughout. Long-range electrostatics were calculated using the Particle Mesh Ewald (PME) method with a cut-off of 11 Å. Bond lengths involving hydrogen atoms were constrained using the SHAKE algorithm, allowing for a 2 fs integration time step. Two independent 500-ns production runs were performed, resulting in a total sampling time of 1 µs. Trajectory analysis was conducted using Python3 scripts. Distances between key arginine side chains and the Neu5Ac residues of GT1b were calculated frame by frame using VMD. Occupancy was defined as the percentage of frames in which the atomic distance remained below 5 Å. All plots were generated using Matplotlib and Seaborn.

Flow cytometry

Human T cells ($1x10^6$) were collected on day 12 after activation with CD3/CD28 Dynabeads (11131D, Thermo Fisher). For evaluation of Siglec-10 binding to T cells, activated T cells were collected, washed with 1xPBS pH 7.4, and incubated with 8 µg/mL of Siglec-10Fc for 30 min at 4 °C. Cells where then washed with 1xPBS pH 7.4 at 450g for 5min, and incubated with anti-CD4 BUV395 (563550, BD Biosciences; 1:800) anti-CD8 APC/H7 (566855, BD Biosciences; 1:800), and anti-human IgG1Fc PE (12-4998-82, Thermo Fisher; 1:2500) for 30 min at 4 °C in the dark. In the case of CD24 detection, the anti-CD24 FITC (MHCD2401, ThermoFisher) was used at 1:250 for 30 mins on ice in the dark. After washing, cells were resuspended in 200 µL staining buffer containing DAPI (1:40,000) (D1306, Invitrogen) before acquisition in FACSymphony (BD Biosciences). Results were analyzed with FlowJo (BD Biosciences).

To investigate the sialic acid linkage dependency of Siglec10-Fc ligand binding on CD4+and CD8+T cells, spleens were harvested from C57BL/6J and sialyltransferase-deficient mice, ST6Gal1fl/flxCD4cre, ST3Gal1, and ST3Gal4, and processed into cell suspensions. Spleens

were macerated in RPMI-1640 medium containing 2% FBS and filtered through a 40 µm mesh. Red blood cells were lysed using ammonium-chloride-potassium (ACK) buffer for 5 minutes at 4°C. Cells were washed and resuspended in HBSS containing either 2% FBS. Cells were stained on ice for 30 minutes using fluorophore-conjugated antibodies listed in the key material table. Siglec10-Fc, pre-complexed following a previously described protocol47, was incubated with the cell suspension to assess binding. After staining, cells were washed and resuspended in flow buffer supplemented with 1 µg/mL 7-AAD (cat# 420403, Biolegend) for viability assessment. Flow cytometric analysis was conducted on a BD Fortessa X-20 cytometer. CD4+T and CD8+T cell populations were gated B220-, CD3+, CD4+ and B220-, CD3+, CD8+ individually. The antibodies used for this experiment were rat anti-mouse B220 (clone:RA3-6B2) (cat# 563793 RRID: AB_2738427, BD Biosciences), rat anti-mouse CD3 (clone: 17A2) (cat# 100231; RRID: AB_11218805, BD Biolegend), rat anti-mouse CD4 (clone: GK1.5) (cat# 612952; RRID: AB_2813886, BD Biosciences), and mouse anti-mouse CD8a (clone: QA17A07) (cat# 155021; RRID: AB_2890707, BD Biolegend).

The breast cancer and U937 cell lines were stained according to a previously described protocol[59]. Briefly, the cells (1 x 10^5) were collected and washed with 1 x PBS pH 7.4. The cells were then stained with Siglec-10Fc complexed with a secondary anti-human IgG1 antibody (A-21445 ThermoFisher or 12-4998-82, Thermo Fisher). The cells were incubated for 45 mins at 4 °C in the dark, prior to being washed with 1 x PBS pH 7.4. The cells were then analyzed by either a Fortessa X-20 (BD Bioscience) or FACSymphony (BD Bioscience) flow cytometer. Data was analyzed using FlowJo software (BD Bioscience).

Siglec-10 blocking experiments were carried out either with S10A IgG4 produced in house, or anti-CD24 blocking SN3 antibody (MA5-11828, ThermoFisher). Either of the antibodies were used at 10 µg/mL and incubated with human T cells or breast cancer cell lines for 30mins, prior to washing the cells with 1x PBS pH7.4. Siglec-10Fc (8 µg/mL) was then precomplexed with anti-IgG1 Fc PE (12-4998-82, ThermoFisher; 1:2500) and incubated for 45 mins on ice in the dark. Cells were washed, stained with DAPI (1:40000) (D1306, Invitrogen) and analyzed on FACSymphony (BD Bioscience). Data was analysed using FlowJo software (BD Bioscience).

Desilalylation and deglycosylation of T cells

For sialic acid cleavage from T cells, human T cells (1 × 10^6) were harvested 12 days post activation and incubated with 50µL of α2-3,6,8,9 Neuraminidase A (P0722, NEB) or α2-3

Neuraminidase S (P0743L, NEB) at 37 °C for 1 h. For global deglycosylation, activated T cells (1×10^6) were treated with 50µL of Protein Deglycosylation Mix II (P6044, NEB) and incubated at 37 °C for 30 min according to manufacturer's instructions. Deglycosylation efficiency was determined by lectin binding as described above.

Antibody internalization

10µg/mL of S10A IgG4 was labelled with pHrodo deep red TFP Ester Dye (P35358, Invitrogen) according to manufacturer's instructions. THP-1-CD19 cells (2×10^5) were collected and washed with 1x PBS pH 7.4 for 5mins at 450g. Portion of the cells was incubated for 1h at 37°C with 10 µM cytochlalasin D (PHZ1063, ThermoFisher). Next, the cells were incubated with the labelled antibody at three different timepoints (0, 10, 30 mins and 30mins + Cyt D) at 4°C. The stained cells were then washed once with 1x PBS pH 7.4 for 5mins at 450g. After washing, cells were resuspended in 200 µL staining buffer containing DAPI (1:40,000) (D1306, Invitrogen) before acquisition in FACSymphony (BD Biosciences). Results were analyzed with FlowJo (BD Biosciences).

For confocal microscopy the sample preparation was the same as above. Cells were then cytospined onto slides using EZ Single Cytofunnel™ , White (Epredia, Cat. #: A78710003) at 800 rpm for 5 minutes. The slides with adhered cells were fixed with 4% paraformaldehyde (PFA) for 15 minutes at room temperature and washed with 1x PBS pH 7.4. Subsequently, cells were stained with DAPI and mounted using ProLong Gold Antifade Reagent (Thermo Fisher Scientific, Cat. #: P3693). Imaging was performed using a Leica SP8 Lightning confocal microscope.

Acknowledgments

This work was supported by the European Research Council (788143-RECGLYCANMR to J.J.-B; ERC-2018-StG 804236-NEXTGEN-IO to A.P.) and the Marie-Skłodowska-Curie actions (ITN Glytunes grant agreement No 956758 to K.S.; and ITN DIRNANO grant agreement No 956544 to F.C.). X-ray diffraction experiments described in this paper were performed using beamlines DLSI04 at Diamond synchrotron (UK). The NMR spectrometers are part of the National NMR Network (PTNMR) and are partially supported by Infrastructure Project No 22161 (co-financed by FEDER through COMPETE 2020, POCI and PORL and FCT through PIDDAC). J.J.-B. and J.E.-O.acknowledge to the European funding for the

GLYCOTwinning project (No. 101079417). A.P.'s research is funded by "La Caixa" Foundation (HR21-00925), AECC (LABAE211744PALA), Fundación FERO, Ikerbasque, and BIOEF EITB MARATOIA BIO19/CP/002. We thank Agencia Estatal de Investigación of Spain for grants PID2019-107956RA-I00 (A.P.), PID2019-107770RA-I00 (J.E.-O.), CONSOLIDACION, RTI2018-099592-B-C21 (F.C.), ID2020-114178GB (R.B. and J.D.S.), RYC2018-024183-I (A.P.), and the Severo Ochoa Center of Excellence Accreditation CEX2021-001136-S, all funded by MCIN/AEI/10.13039/501100011033 and by El FSE invierte en tu futuro, as well as CIBERES, and initiative of Instituto de Salud Carlos III (ISCIII, Spain) A.A.-V. receives funding from "La Caixa" Foundation (ID 100010434, LCF/BQ/DR20/11790022). A. B. (AECC Bizkaia Scientific Foundation, PRDVZ19003BOSC). F.C. and JEO acknowledges the Mizutani Foundation for Glycoscience (Grants 220115 and 250082, respectively); and J.E.O. Caixa Junior Leader, BBVA Fundación for Leonardo Grant and Ramón Areces Fundation. A. G. thanks Agencia Estatal de Investigación of Spain for grants PID2023-150779OA-I00 and RYC2022-037985-I. A. T thanks Europe Marie Skłodowska-Curie Doctoral Networks (MSCA-DN) actions (Grant Agreement 101119499). We thank Prof Rob Field and Iakovia Ttoffi for the 3'SL and 6'SL ligands provided. For the ST3Gal1-/- and ST3Gal4-/- mice, we acknowledge Jamey Marth (Sanford Burnham Prebys Medical Discovery Institute, Infectious and Inflammatory Diseases, USA). IT Solutions at the University of Southampton is gratefully acknowledged for the generous allocation of computational resources on the HPC cluster Iridis. The Science Foundation of Ireland (SFI) Frontiers for the Future Programme is gratefully acknowledged for financial support of SDA postgraduate training (20/FFP-P/8809). The opinions, findings, and conclusions or recommendations expressed in this material are those of the author(s) and do not necessarily reflect the views of the Science Foundation of Ireland.

Data availability

The crystalographic data of Siglec-10–S10A Fab complex alone and in complex with 6´SL generated in this study have been deposited in the Protein Data Bank database under accession codes 9R7P and 9R8E. Molecular dynamics simulations data, along with the top 10 poses from AutoDock Vina for Siglec-10, have been deposited in the "open science framework" repository and can be accessed at the following link: https://osf.io/ykgf5/?view_only=21f8c01e396b456dadba577a842f49d9. Any remaining

information can be obtained from the corresponding author upon request. Source data are provided with this paper.

Conflict of interest

The authors declare no conflict of interest.

Figures

Figure 1. Overall structure of human Siglec-10 in complex with S10A Fab. a) Surface representation of the crystal structure of Siglec-10 with V-Ig domain in purple and C2-Ig domain in blue. Canonical arginine R119 is represented as a red sphere and the conserved N100 glycan as blue sticks. A grey mesh represents the composite omit electron density map (1.0 σ contour level) associated with N100 glycan. b) Surface and cartoon representation of Siglec-10 in complex with anti-Siglec-10 S10A Fab. S10A is composed of a heavy chain (HC) (in dark grey) and a light chain (LC) (in light grey). The variable (VH and VL) region of S10A Fab binds to the V-Ig domain of Siglec-10 (in purple). Zoomed in are the residues involved in Siglec-10 binding of the CDRs of S10A Fab HC (top) and LC (bottom). c**)** Cartoon representation of Siglec-10 V-Ig domain (in purple) with 6'SL represented as sticks with Neu_5Ac in pink and Gal in yellow, the Glc moiety is missing due to lack of direct contact with Siglec-10. A grey mesh represents the composite omit electron density map (1.0 σ contour level) associated with Neu_5Ac and Gal sugar moieties. Highlighted are the residues involved in polar interactions between Siglec-10 and 6'SL. d**)** 2D interaction diagram highlighting the key intermolecular contacts responsible for the interactions between Siglec-10 and the 6'SL.

Figure 2. Molecular recognition of 6′SL, 3′SL and 6-*S*-6'-*S*-3'SLN by Siglec-10. a) STD-NMR based epitope mapping for 6′SL, 3′SL and 6-*S*-6'-*S*-3'SLN in the presence of Siglec-10. The relative STD response is coded according to the legend. b) STD-NMR spectra of WT and mutant forms of Siglec-10Fc binding to 6'SL with a molar ratio of 1:100 (Siglec-10:ligand). Reference off-resonance spectrum in black, Siglec-10Fc WT in blue, Siglec-10Fc R127A in red, Siglec-10Fc R119A in pink, Siglec-10Fc R119/127A in green and the IgG1Fc negative control in orange.

Figure 3. Siglec-10 binding to human cell lines measured by flow cytometry. a) Pooled data of Siglec-10Fc binding after complete de-glycosylation (Deglyco) treatment of human CD8+ and CD4+ T cells (n = 4 donors). b) Pooled data of Siglec-10Fc binding after desialylation with Neuraminidase A (Neu A) of human CD8+ and CD4+ T cells (n = 4 donors). c) Binding of Siglec-10Fc to human CD8+ and CD4+ T cells treated with Neuraminidase S (Neu S) (n = 3/4 donors). d) Pooled data of Siglec-10Fc WT binding to ST3Gal1$^{-/-}$, ST3Gal4$^{-/-}$ and ST6Gal1$^{-/-}$ murine T cells (n=3 donors) e) Siglec-10Fc WT and mutant proteins binding to CD4+ and CD8+ human T cells (n = 4 donors). f) Right – cartoon representation of the generation of the CMAS KO U937 cell line. Left – Pooled data representing the effect of CMAS KO on Siglec-10Fc WT binding (n = 4 donors). g) Right – Cartoon representation of the CHST1 and CHST2 overexpression to increase cell surface sulfation. Left – Siglec-10Fc WT binding (n = 4 donors). Error bars denote SEM as determined by two-tailed, unpaired Student's t test.

Figure 4. GT1b ganglioside in complex with Siglec-10. a) Left panel: 3D model of the Siglec-10/GT1b complex used for the MD simulations. The protein was rendered with transparent surface and cartoon in light blue to highlight secondary structure motifs. The GT1b ganglioside rendered with sticks with C atoms in tan, O in red, and N in blue. The three Neu5Ac are labelled according to their linkages (α2-3 terminal, α2-3 internal, and α2-8). Right panel: Representative frame from the MD simulation showing a rearranged binding conformation. The R127 shift its interaction to the terminal α2-3 Neu5Ac, while R119 maintains its interaction with the α2-8 Neu5Ac. b) Distance plots showing the interactions between Siglec-10 arginine residues and the Neu5Ac moieties of GT1b over 500 ns (MD1) (top) and 400 ns (MD2) (bottom). The red dashed line at 5 Å indicates the threshold distance for interaction. c) Occupancy analysis for the interactions between Arg and Neu5Ac residues in MD1 (top) and MD2 (bottom), respectively. Occupancy is defined as the percentage of simulation frames where the interatomic distance remains below 5 Å. MD1 shows dominant occupancy for R119 α2-8 (95.8%) and R127 α2-3 terminal (77.0%). In MD2, R119 switches preference, with 71.6% occupancy toward α2-3 terminal, and R127 shows a strong preference for α2-3 internal (92.8%).

Figure 5. Flow cytometric analysis of CD24 expression and Siglec-10 binding across human cells. a) Quantitative summary of CD24 expression and Siglec-10 interactions across MCF7, MDA-MB-231, MDA-MB-468, T47D, and SKBR3 breast cancer cell lines. b) Representative histograms demonstrating Siglec-10 binding to two CD24-expressing breast cancer cell lines in the absence (blue) or presence (purple) of a blocking anti-CD24 monoclonal

antibody (mAb). c) Left- Representative histogram of CD24 expression on activated human T cells. Right- Histogram showing Siglec-10 binding to activated T cells with (purple) or without (blue) SN3 anti-CD24 mAb blockade. d) Representative histograms showing CD24 overexpression in Jurkat cells and corresponding Siglec-10 binding to parental (blue) versus CD24-overexpressing (red) Jurkat cells.

Figure 6. Siglec-10 modulates CAR-T cell cytotoxicity. a) Schematic representation of the *in vitro* cytotoxic assay. b) Pooled data showing the impact of Siglec-10 expression on CAR-T cell cytotoxicity compared to parental THP-1 cell line (n= 3 donors). c) Representative histograms illustrating S10A IgG4 blockade of Siglec-10 interactions on activated human CD4+ and CD8+ T cells. d) Confocal microscopy images depicting S10A IgG4 internalization in THP-1 cells with or without endocytosis inhibition by CyD, at different time points. e) Pooled quantification of S10A IgG4 internalization in THP-1 cells under the same conditions measured by flow cytometry (n= 2 donors). f) Pooled data showing the effect of S10A IgG4 mAb treatment on CAR-T cytotoxicity in the presence (left) or absence (right) of Siglec-10 expression (n= 3 donors). Error bars represent SEM; statistical significance was determined by two-tailed, unpaired Student's t test.

References

1. Granovsky, M. *et al.* Suppression of tumor growth and metastasis in Mgat5-deficient mice. *Nat. Med.* **6**, 306–312 (2000).
2. Munkley, J. & Elliott, D. J. Hallmarks of glycosylation in cancer. *Oncotarget* **7**, 35478–35489 (2016).
3. Pinho, S. S. & Reis, C. A. Glycosylation in cancer: mechanisms and clinical implications. *Nat. Rev. Cancer* **15**, 540–555 (2015).
4. RodrÍguez, E., Schetters, S. T. T. & van Kooyk, Y. The tumour glyco-code as a novel immune checkpoint for immunotherapy. *Nat. Rev. Immunol.* **18**, 204–211 (2018).
5. van Houtum, E. J. H., Büll, C., Cornelissen, L. A. M. & Adema, G. J. Siglec Signaling in the Tumor Microenvironment. *Front. Immunol.* **12**, (2021).
6. Mantuano, N. R. & Läubli, H. Sialic acid and Siglec receptors in tumor immunity and immunotherapy. *Semin. Immunol.* **74–75**, 101893 (2024).
7. Jiang, K.-Y., Qi, L.-L., Kang, F.-B. & Wang, L. The intriguing roles of Siglec family members in the tumor microenvironment. *Biomark. Res.* **10**, 22 (2022).

8. Paulson, J. C., Macauley, M. S. & Kawasaki, N. Siglecs as sensors of self in innate and adaptive immune responses. *Ann. N. Y. Acad. Sci.* **1253**, 37–48 (2012).
9. Macauley, M. S., Crocker, P. R. & Paulson, J. C. Siglec-mediated regulation of immune cell function in disease. *Nat. Rev. Immunol.* **14**, 653–666 (2014).
10. Forgione, R. E. *et al.* Unveiling Molecular Recognition of Sialoglycans by Human Siglec-10. *iScience* **23**, (2020).
11. Whitney, G. *et al.* A new siglec family member, siglec-10, is expressed in cells of the immune system and has signaling properties similar to CD33. *Eur. J. Biochem.* **268**, 6083–6096 (2001).
12. Wang, C. *et al.* Identification of Siglec-10 as a new dendritic cell checkpoint for cervical cancer immunotherapy. *J. Immunother. Cancer* **12**, e009404 (2024).
13. Demoulin, S. A. *et al.* Cervical (pre)neoplastic microenvironment promotes the emergence of tolerogenic dendritic cells via RANKL secretion. *OncoImmunology* **4**, e1008334 (2015).
14. Duan, S. & Paulson, J. C. Siglecs as Immune Cell Checkpoints in Disease. *Annu. Rev. Immunol.* **38**, 365–395 (2020).
15. Barkal, A. A. *et al.* CD24 signalling through macrophage Siglec-10 is a target for cancer immunotherapy. *Nature* **572**, 392–396 (2019).
16. Meyer, S. J., Linder, A. T., Brandl, C. & Nitschke, L. B Cell Siglecs–News on Signaling and Its Interplay With Ligand Binding. *Front. Immunol.* **9**, (2018).
17. OncoC4 Announces First Patient Dosed in Phase 1 Trial for Novel SIGLEC10 Immune Checkpoint Inhibitor ONC-841 for Solid Tumors | OncoC4. https://oncoc4.com/press-releases/oncoc4-announces-first-patient-dosed-in-phase-1-trial-for-novel-siglec10-immune-checkpoint-inhibitor-onc-841-for-solid-tumors/ (2024).
18. Rapoport, E., Mikhalyov, I., Zhang, J., Crocker, P. & Bovin, N. Ganglioside binding pattern of CD33-related siglecs. *Bioorg. Med. Chem. Lett.* **13**, 675–678 (2003).
19. Lenza, M. P. *et al.* Structural insights into Siglec-15 reveal glycosylation dependency for its interaction with T cells through integrin CD11b. *Nat. Commun.* **14**, 3496 (2023).
20. Blixt, O., Collins, B. E., Nieuwenhof, I. M. van den, Crocker, P. R. & Paulson, J. C. Sialoside Specificity of the Siglec Family Assessed Using Novel Multivalent Probes: IDENTIFICATION OF POTENT INHIBITORS OF MYELIN-ASSOCIATED GLYCOPROTEIN *. *J. Biol. Chem.* **278**, 31007–31019 (2003).

21. Chen, G.-Y. *et al.* Preserving Sialic Acid-dependent Pattern Recognition by CD24-Siglec G Interaction for Therapy of Polybacterial Sepsis. *Nat. Biotechnol.* **29**, 428–435 (2011).
22. Chen, G.-Y., Tang, J., Zheng, P. & Liu, Y. CD24 and Siglec-10 Selectively Repress Tissue Damage-Induced Immune Responses. *Science* **323**, 1722–1725 (2009).
23. Bandala-Sanchez, E. *et al.* CD52 glycan binds the proinflammatory B box of HMGB1 to engage the Siglec-10 receptor and suppress human T cell function. *Proc. Natl. Acad. Sci. U. S. A.* **115**, 7783–7788 (2018).
24. Ma, S. *et al.* Enzyme-Sialylation-Controlled Chemical Sulfation of Glycan Epitopes for Decoding the Binding of Siglec Ligands. *J. Am. Chem. Soc.* **146**, 29469–29480 (2024).
25. Jung, J., Schmidt, E. N. & Macauley, M. S. Carbohydrate sulfation as a critical modulator of siglec-sialoglycan interactions. *Carbohydr. Res.* **553**, 109502 (2025).
26. CORNEN, S., Gauthier, L., Rossi, B. & Wagtmann, N. Siglec-10 antibodies. (2017).
27. Lenza, M. P., Atxabal, U., Oyenarte, I., Jiménez-Barbero, J. & Ereño-Orbea, J. Current Status on Therapeutic Molecules Targeting Siglec Receptors. *Cells* **9**, 2691 (2020).
28. Ereño-Orbea, J. *et al.* Structural Basis of Enhanced Crystallizability Induced by a Molecular Chaperone for Antibody Antigen-Binding Fragments. *J. Mol. Biol.* **430**, 322–336 (2018).
29. Ereño-Orbea, J. *et al.* Molecular basis of human CD22 function and therapeutic targeting. *Nat. Commun.* **8**, 764 (2017).
30. Pronker, M. F. *et al.* Structural basis of myelin-associated glycoprotein adhesion and signalling. *Nat. Commun.* **7**, 13584 (2016).
31. Krissinel, E. & Henrick, K. Inference of macromolecular assemblies from crystalline state. *J. Mol. Biol.* **372**, 774–797 (2007).
32. Alphey, M. S., Attrill, H., Crocker, P. R. & van Aalten, D. M. F. High resolution crystal structures of Siglec-7. Insights into ligand specificity in the Siglec family. *J. Biol. Chem.* **278**, 3372–3377 (2003).
33. Crocker, P. R., Paulson, J. C. & Varki, A. Siglecs and their roles in the immune system. *Nat. Rev. Immunol.* **7**, 255–266 (2007).
34. Lenza, M. P. *et al.* Structures of the Inhibitory Receptor Siglec-8 in Complex with a High-Affinity Sialoside Analogue and a Therapeutic Antibody. *JACS Au* **3**, 204–215 (2023).

35. Jumper, J. *et al.* Highly accurate protein structure prediction with AlphaFold. *Nature* **596**, 583–589 (2021).
36. Jung, J. *et al.* Carbohydrate Sulfation As a Mechanism for Fine-Tuning Siglec Ligands. *ACS Chem. Biol.* **16**, 2673–2689 (2021).
37. Schmidt, E. N. *et al.* Siglec-6 mediates the uptake of extracellular vesicles through a noncanonical glycolipid binding pocket. *Nat. Commun.* **14**, 2327 (2023).
38. Chen, G.-Y., Tang, J., Zheng, P. & Liu, Y. CD24 and Siglec-10 Selectively Repress Tissue Damage-Induced Immune Responses. *Science* **323**, 1722–1725 (2009).
39. Zhang, X., Yu, C., Liu, J.-Q. & Bai, X.-F. Dendritic cell expression of CD24 contributes to optimal priming of T lymphocytes in lymph nodes. *Front. Immunol.* **14**, (2023).
40. Shi, Y. *et al.* CD24 is expressed on FoxP3+ regulatory T cells and regulates their function. *Am. J. Transl. Res.* **14**, 2291–2300 (2022).
41. Li, O., Zheng, P. & Liu, Y. CD24 Expression on T Cells Is Required for Optimal T Cell Proliferation in Lymphopenic Host. *J. Exp. Med.* **200**, 1083–1089 (2004).
42. Yamakawa, N. *et al.* Discovery of a new sialic acid binding region that regulates Siglec-7. *Sci. Rep.* **10**, 8647 (2020).
43. Daly, J., Piatnitca, L., Al-Seragi, M., Krishnamoorthy, V. & Wisnovsky, S. CRISPR activation screens map the genomic landscape of cancer glycome remodeling. 2025.05.26.656133 Preprint at https://doi.org/10.1101/2025.05.26.656133 (2025).
44. Chen, G.-Y., Tang, J., Zheng, P. & Liu, Y. CD24 and Siglec-10 Selectively Repress Tissue Damage–Induced Immune Responses. *Science* **323**, 1722–1725 (2009).
45. DeBono, N. J. *et al.* The molecular basis of immunosuppression by soluble CD52 is defined by interactions of N-linked and O-linked glycans with HMGB1 box B. *J. Biol. Chem.* **301**, 108350 (2025).
46. McCord, K. A. *et al.* Dissecting the Ability of Siglecs To Antagonize Fcγ Receptors. *ACS Cent. Sci.* **10**, 315–330 (2024).
47. Khuvis, S. *et al.* Optimizing Amber for Device-to-Device GPU Communication. in *Practice and Experience in Advanced Research Computing 2023: Computing for the Common Good* 200–205 (Association for Computing Machinery, New York, NY, USA, 2023). doi:10.1145/3569951.3597553.
48. Hornak, V. *et al.* Comparison of multiple Amber force fields and development of improved protein backbone parameters. *Proteins Struct. Funct. Bioinforma.* **65**, 712–725 (2006).

49. Kirschner, K. N. *et al.* GLYCAM06: a generalizable biomolecular force field. Carbohydrates. *J. Comput. Chem.* **29**, 622–655 (2008).

50. Jumper, J. *et al.* Highly accurate protein structure prediction with AlphaFold. *Nature* **596**, 583–589 (2021).

51. Jorgensen, W. L., Chandrasekhar, J., Madura, J. D., Impey, R. W. & Klein, M. L. Comparison of simple potential functions for simulating liquid water. *J. Chem. Phys.* **79**, 926–935 (1983).

52. Berne, B. J. Molecular Dynamics in Systems with Multiple Time Scales: Reference System Propagator Algorithms. in *Computational Molecular Dynamics: Challenges, Methods, Ideas* (eds. Deuflhard, P. et al.) 297–317 (Springer, Berlin, Heidelberg, 1999). doi:10.1007/978-3-642-58360-5_16.

53. Darden, T., York, D. & Pedersen, L. Particle mesh Ewald: An N·log(N) method for Ewald sums in large systems. *J. Chem. Phys.* **98**, 10089–10092 (1993).

54. AlphaFold Protein Structure Database in 2024: providing structure coverage for over 214 million protein sequences | Nucleic Acids Research | Oxford Academic. https://academic.oup.com/nar/article/52/D1/D368/7337620.

55. Singh, eLab memebers, Ojas. GlycoShape. https://glycoshape.org/.

56. Ives, C. M. *et al.* Restoring protein glycosylation with GlycoShape. *Nat. Methods* **21**, 2117–2127 (2024).

57. Jo, S., Kim, T., Iyer, V. G. & Im, W. CHARMM-GUI: a web-based graphical user interface for CHARMM. *J. Comput. Chem.* **29**, 1859–1865 (2008).

58. Lee, J. *et al.* CHARMM-GUI Input Generator for NAMD, GROMACS, AMBER, OpenMM, and CHARMM/OpenMM Simulations Using the CHARMM36 Additive Force Field. *J. Chem. Theory Comput.* **12**, 405–413 (2016).

59. Schmidt, E. N., Jung, J. & Macauley, M. S. Flow Cytometry-Based Detection of Siglec Ligands. in *Carbohydrate-Protein Interactions: Methods and Protocols* (eds. Abbott, D. W. & Zandberg, W. F.) 181–193 (Springer US, New York, NY, 2023). doi:10.1007/978-1-0716-3151-5_13.

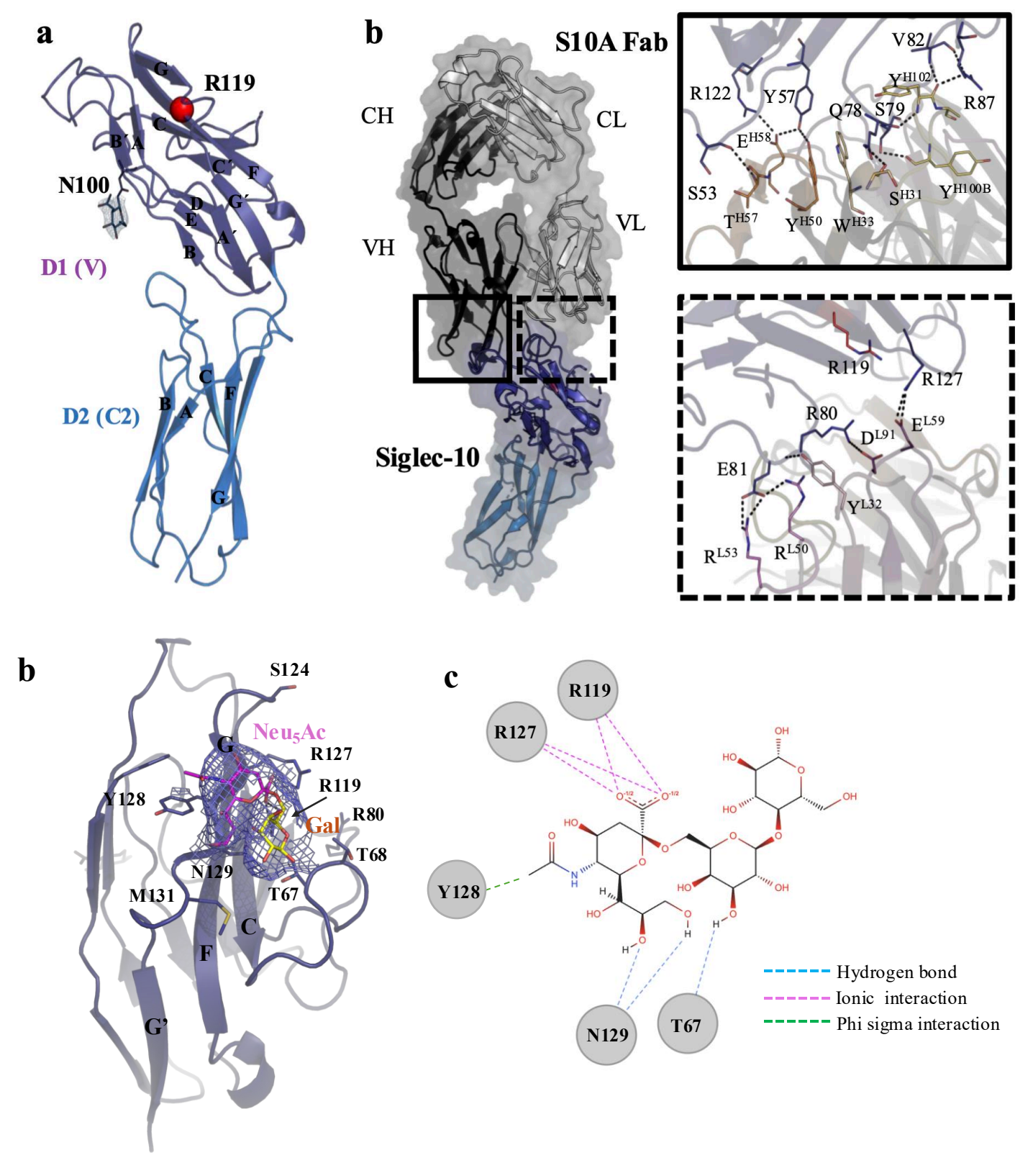
a
R119
N100
D1 (V)
D2 (C2)
b
S10A Fab
CH
CL
VH
VL
Siglec-10
R122
Y57
V82
YH102
Q78
S79
R87
EH58
S53
SH31
YH100B
THH57
YH50
WH33
R119
R127
R80
EL59
DL91
E81
YL32
RL53
RL50
b
S124
Neu5Ac
R127
R119
Y128
R80
Gal
T68
N129
M131
T67
c
R119
R127
Y128
N129
T67
Hydrogen bond
Ionic interaction
Phi sigma interaction

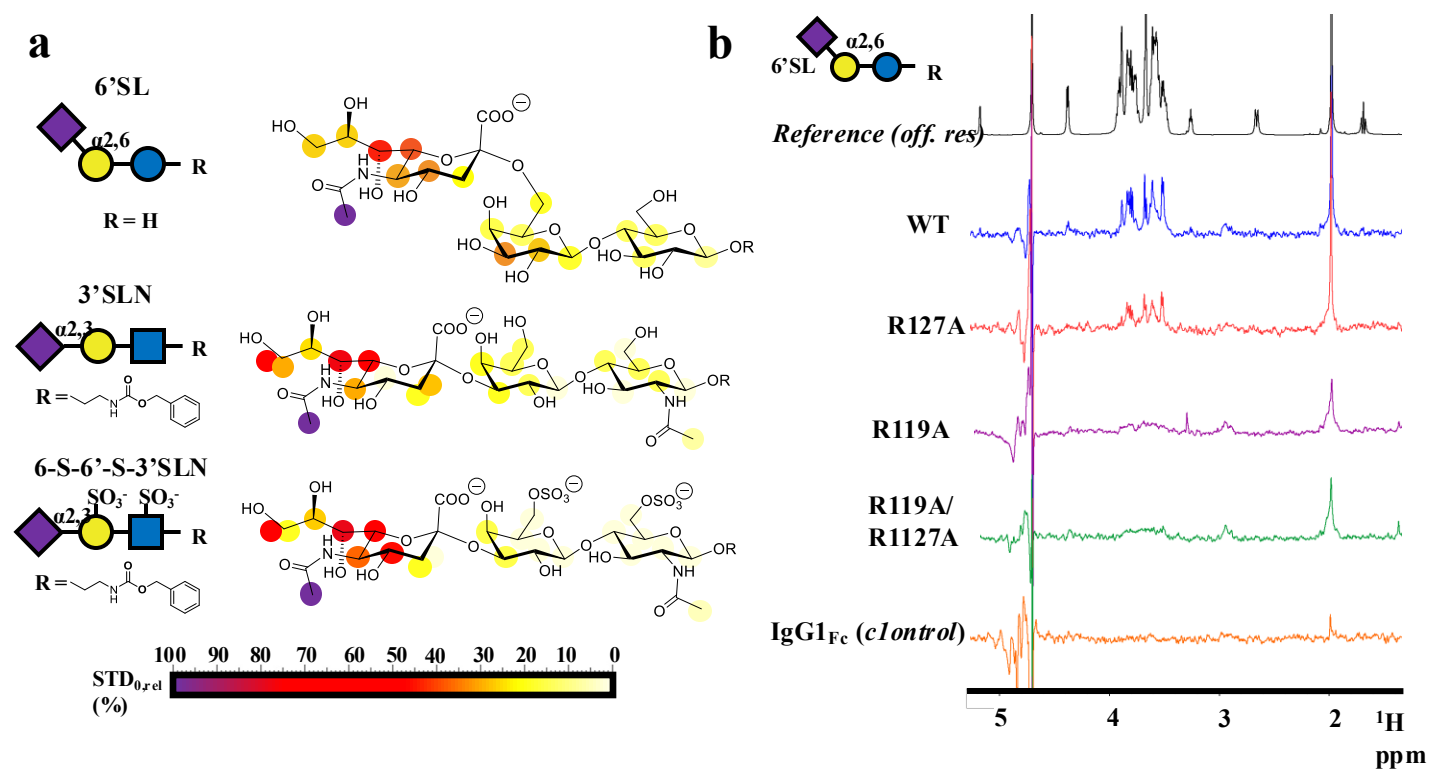
a
6'SL
α2,6
R
R = H
3'SLN
α2,3
R
R =
6-S-6'-S-3'SLN
SO3- SO3-
α2,3
R
R =
100 90 80 70 60 50 40 30 20 10 0
STD0,rel
(%)
b
6'SL
α2,6
R
Reference (off. res)
WT
R127A
R119A
R119A/
R1127A
IgG1Fc (c1ontrol)
5 4 3 2 1H
ppm

Fig3

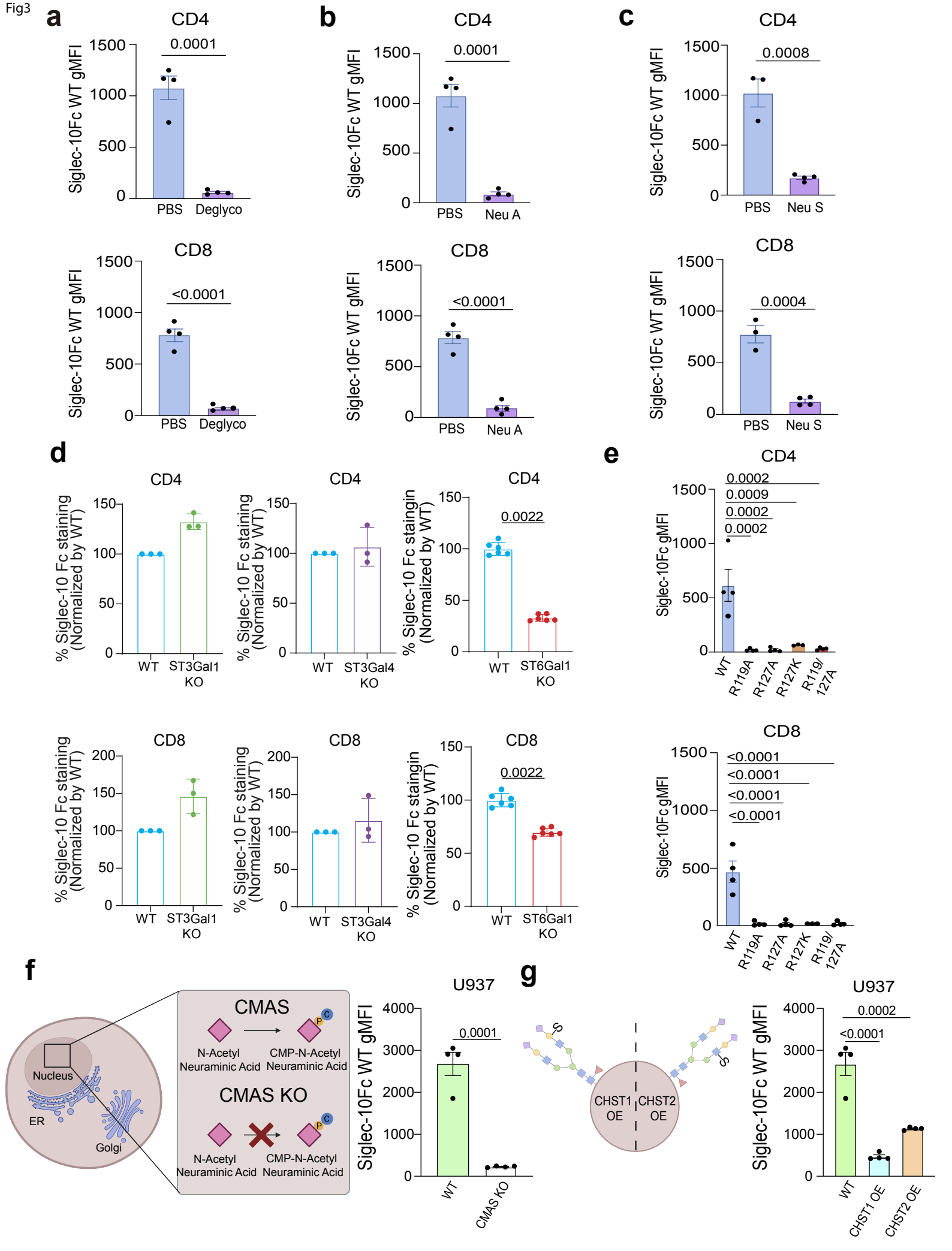
a
CD4
Siglec-10Fc WT gMFI
0.0001
PBS
Deglyco
CD8
<0.0001
b
Neu A
c
Neu S
0.0008
0.0004
d
% Siglec-10 Fc staining (Normalized by WT)
WT
ST3Gal1 KO
ST3Gal4 KO
ST6Gal1 KO
0.0022
e
Siglec-10Fc gMFI
R119A
R127A
R127K
R119/ 127A
0.0002
0.0009
<0.0001
f
Nucleus
ER
Golgi
CMAS
N-Acetyl Neuraminic Acid
CMP-N-Acetyl Neuraminic Acid
CMAS KO
U937
CMAS KO
g
CHST1 OE
CHST2 OE

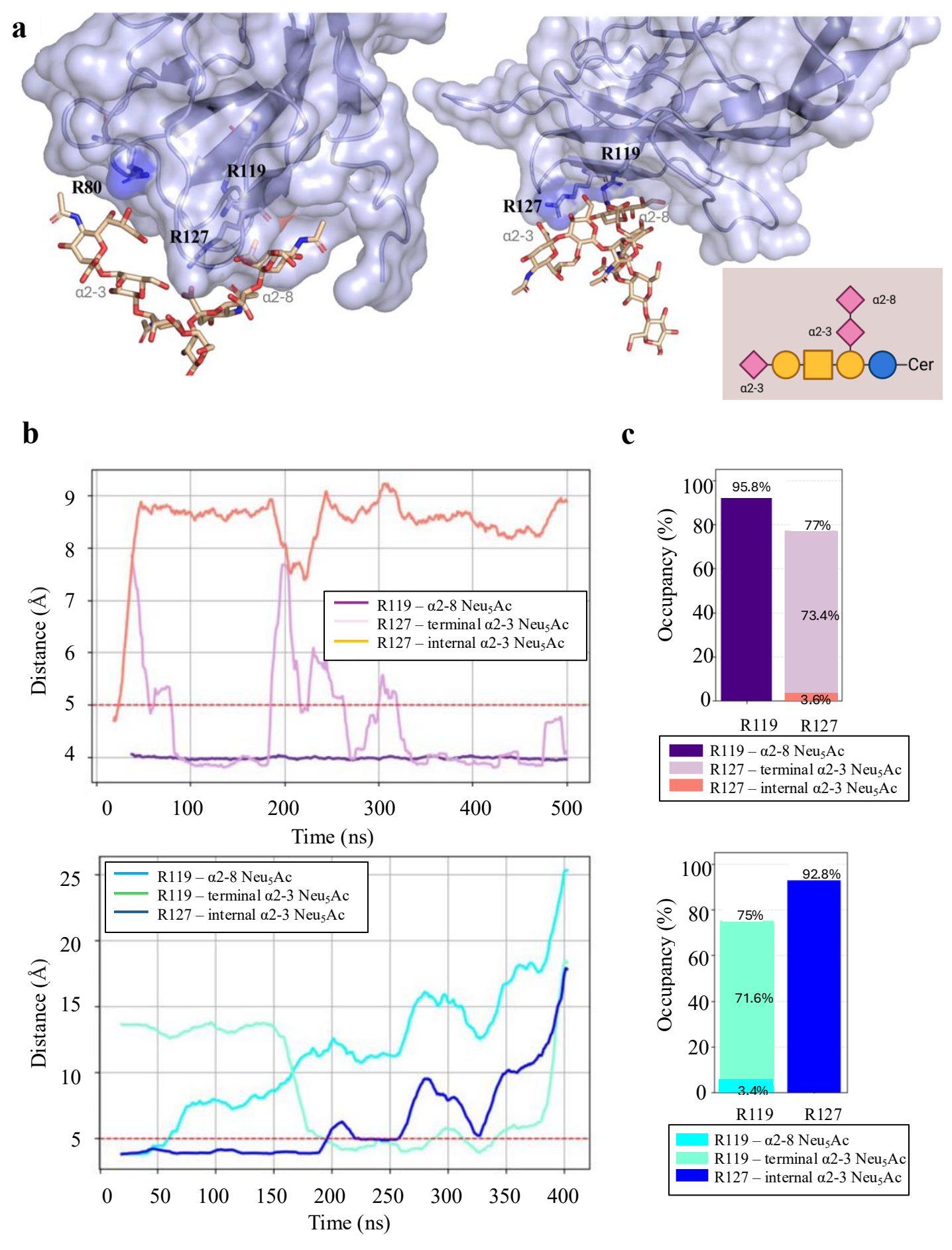
a
R80
R119
R127
α2-3
α2-8
R119
R127
α2-8
α2-3
α2-8
α2-3
Cer
α2-3
b
Distance (Å)
Time (ns)
R119 – α2-8 Neu5Ac
R127 – terminal α2-3 Neu5Ac
R127 – internal α2-3 Neu5Ac
R119 – α2-8 Neu5Ac
R119 – terminal α2-3 Neu5Ac
R127 – internal α2-3 Neu5Ac
c
Occupancy (%)
95.8%
77%
73.4%
3.6%
R119
R127
R119 – α2-8 Neu5Ac
R127 – terminal α2-3 Neu5Ac
R127 – internal α2-3 Neu5Ac
Occupancy (%)
75%
71.6%
3.4%
92.8%
R119
R127
R119 – α2-8 Neu5Ac
R119 – terminal α2-3 Neu5Ac
R127 – internal α2-3 Neu5Ac

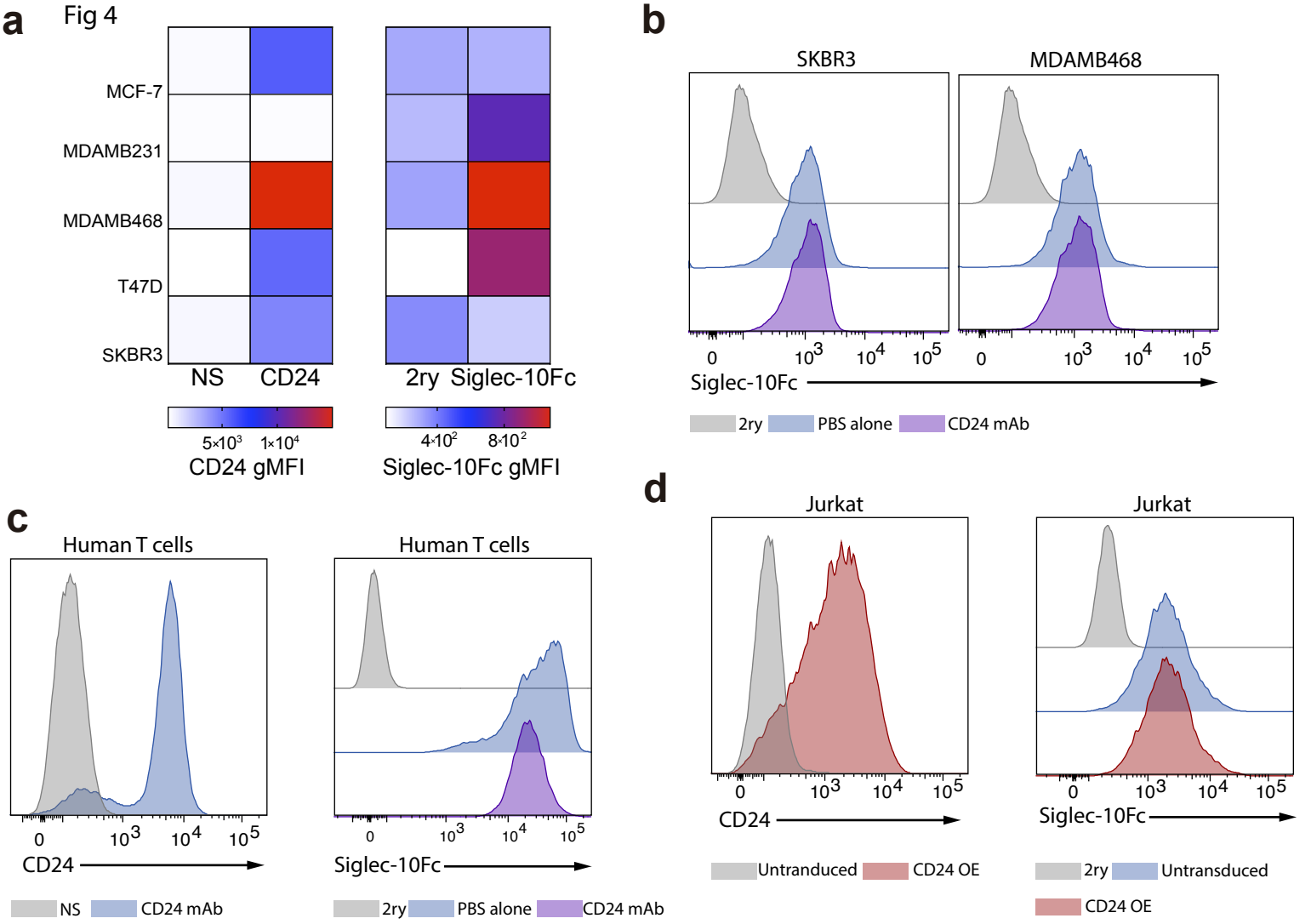
a
Fig 4
MCF-7
MDAMB231
MDAMB468
T47D
SKBR3
NS
CD24
2ry
Siglec-10Fc
5×10³
1×10⁴
CD24 gMFI
4×10²
8×10²
Siglec-10Fc gMFI
b
SKBR3
MDAMB468
0
10³
10⁴
10⁵
Siglec-10Fc
2ry
PBS alone
CD24 mAb
c
Human T cells
Human T cells
CD24
Siglec-10Fc
NS
CD24 mAb
2ry
PBS alone
CD24 mAb
d
Jurkat
Jurkat
CD24
Siglec-10Fc
Untranduced
CD24 OE
2ry
Untransduced
CD24 OE

Fig5

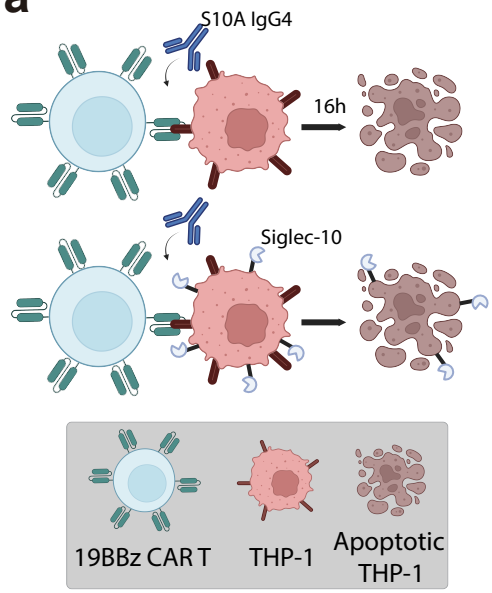
a
S10A IgG4
16h
Siglec-10
19BBz CAR T
THP-1
Apoptotic THP-1

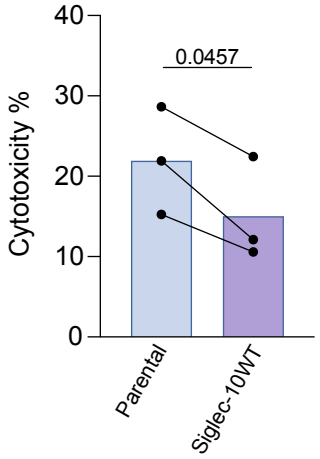
b
Cytotoxicity %
0.0457
Parental
Siglec-10WT

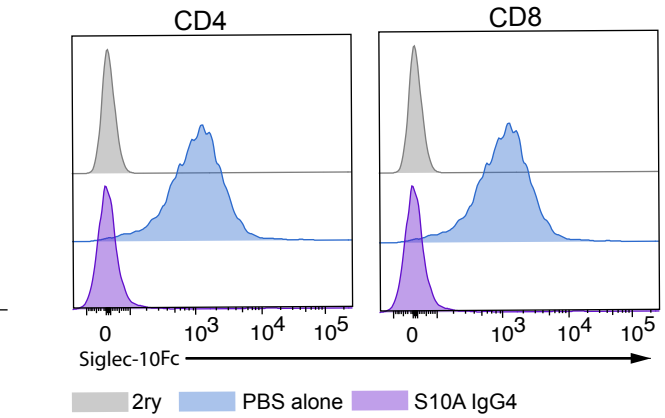
c
CD4
CD8
Siglec-10Fc
2ry
PBS alone
S10A IgG4

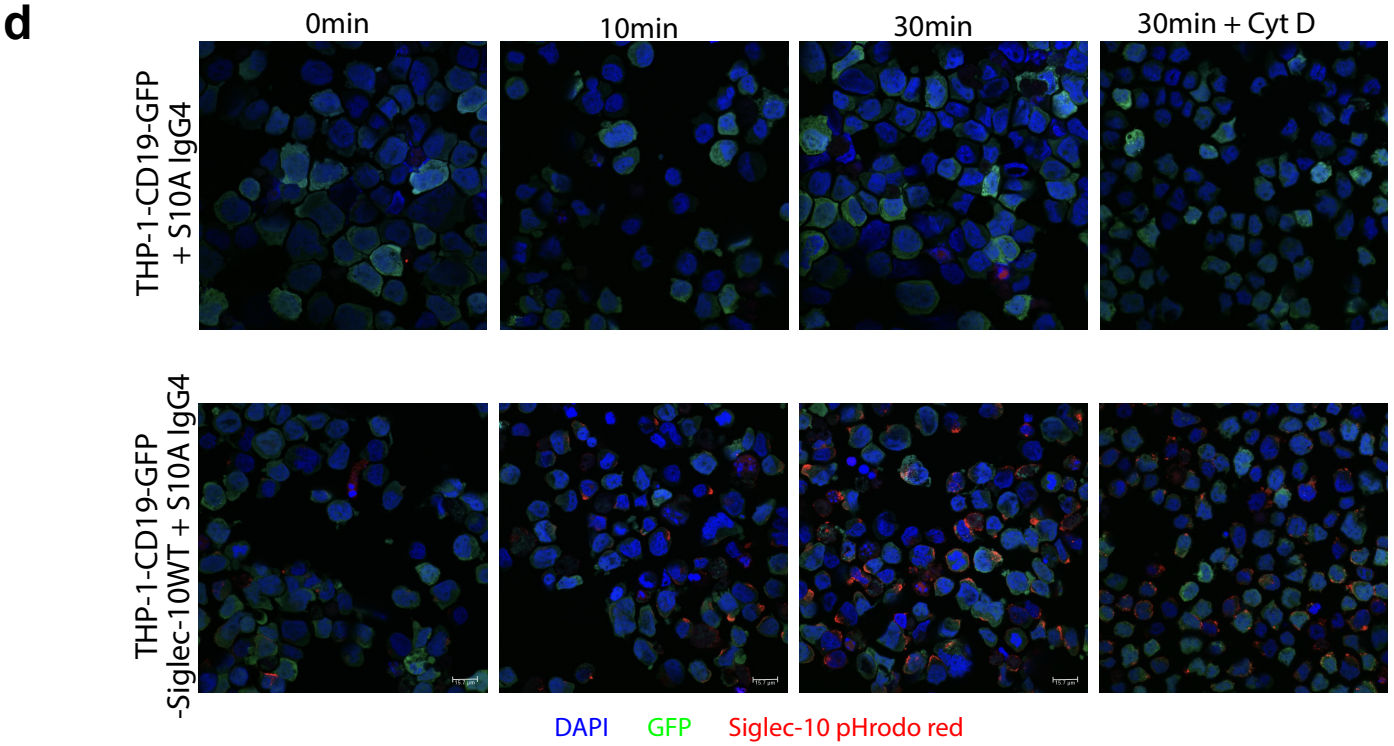
d
0min
10min
30min
30min + Cyt D
THP-1-CD19-GFP + S10A IgG4
THP-1-CD19-GFP -Siglec-10WT + S10A IgG4
DAPI
GFP
Siglec-10 pHrodo red

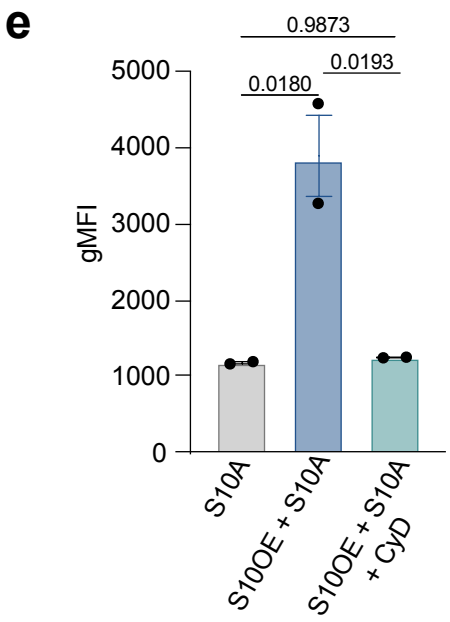
e
gMFI
0.9873
0.0193
0.0180
S10A
S10OE + S10A
S10OE + S10A + CyD

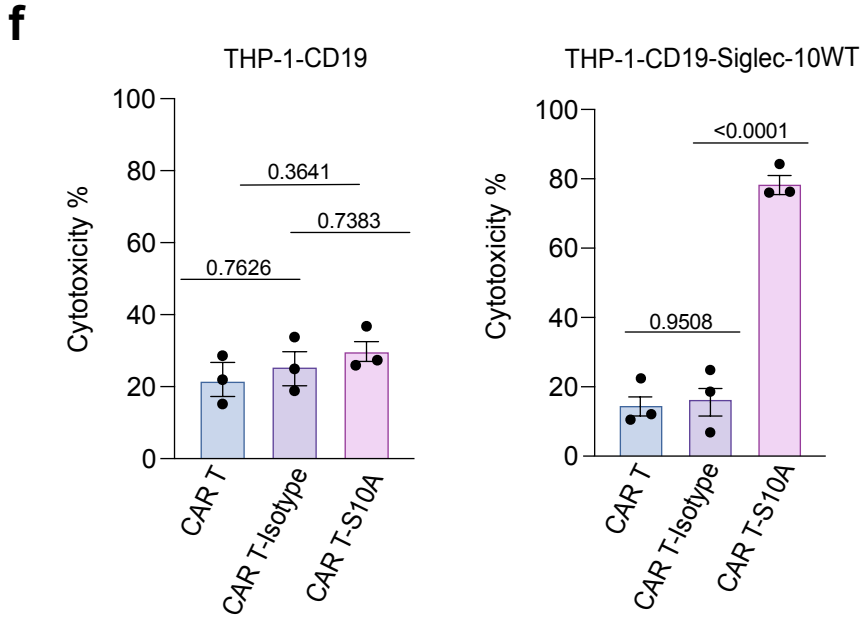
f
THP-1-CD19
THP-1-CD19-Siglec-10WT
Cytotoxicity %
0.3641
0.7383
0.7626
<0.0001
0.9508
CAR T
CAR T-Isotype
CAR T-S10A